

DEC 23 1946

ACR No. L4D19

NATIONAL ADVISORY COMMITTEE FOR AERONAUTICS

WARTIME REPORT

ORIGINALLY ISSUED

April 1944 as

Advance Confidential Report L4D19

COMPARISON OF YAW CHARACTERISTICS OF A SINGLE-ENGINE

AIRPLANE MODEL WITH SINGLE-ROTATING AND

DUAL-ROTATING PROPELLERS

By R. H. Neely, L. E. Fogarty,
and S. R. Alexander

Langley Memorial Aeronautical Laboratory
Langley Field, Va.

NACA

WASHINGTON

NACA LIBRARY
LANGLEY MEMORIAL AERONAUTICAL
LABORATORY
Langley Field, Va.

NACA WARTIME REPORTS are reprints of papers originally issued to provide rapid distribution of advance research results to an authorized group requiring them for the war effort. They were previously held under a security status but are now unclassified. Some of these reports were not technically edited. All have been reproduced without change in order to expedite general distribution.

NATIONAL ADVISORY COMMITTEE FOR AERONAUTICS

ADVANCE CONFIDENTIAL REPORT NO. L4D19

COMPARISON OF YAW CHARACTERISTICS OF A SINGLE-ENGINE
AIRPLANE MODEL WITH SINGLE-ROTATING AND
DUAL-ROTATING PROPELLERS

By R. H. Neely, L. E. Fogarty,
and S. R. Alexander

SUMMARY

Tests were made in the NACA 19-foot pressure tunnel to determine the yaw characteristics of a 0.32-scale model of a single-engine, fighter-type airplane with six-blade single-rotating and dual-rotating propellers. The propellers used in the investigation were of the same solidity and plan form. Force and moment characteristics of the model, with the exception of the rolling-moment characteristics, are presented for several model and power conditions. Curves are given that show estimated rudder-control characteristics of the design airplane in steady sideslips.

The most important difference in the yaw characteristics of the airplane model with single-rotating and dual-rotating propellers was that, in the low-speed high-thrust conditions, large rudder deflections and forces were required to trim at zero yaw with single rotation, and negligible deflections and forces were required to trim at zero yaw with dual rotation. For the high-thrust conditions with the rudder fixed, the model with single-rotating propellers tended to be directionally unstable at large negative angles of yaw; whereas, with dual-rotating propellers the model was stable throughout the trim range. For moderate angles of yaw, a greater degree of rudder-fixed stability was generally obtained with single rotation than with dual rotation. The total range of angle of yaw maintained by maximum deflection of

the rudder was greater with dual rotation. The rudder-control forces per degree of yaw were two to three times as great for single rotation as for dual rotation in the high-thrust conditions.

INTRODUCTION

The effects of propeller operation on the stability and control characteristics of the airplane are becoming increasingly important with the present trend toward engines of greater power. The single-rotating propeller, used almost exclusively in the past, has an adverse effect on the lateral-control characteristics of the airplane. With power on, the large torque reaction and the resulting asymmetrical slipstream causes large lateral-trim changes that involve both aileron and rudder. A dual-rotating propeller, which for the ideal case has no resultant torque and produces a symmetrical slipstream, should eliminate the lateral-control changes due to power. Air-flow surveys at the tail of a single-engine airplane model equipped with a dual-rotating propeller have indicated a symmetrical slipstream (reference 1). It has been shown, however, by theory (reference 2) and by experiment (reference 3) that the propeller forces due to inclination of the thrust axis are greater for a dual-rotating propeller than for a single-rotating propeller; this effect influences the stability of the airplane somewhat.

Little is known about the quantitative differences between the effects of a single-rotating and a dual-rotating propeller on the stability and control characteristics of a complete airplane. In order to provide information on the differences between the effects of a single-rotating and a dual-rotating propeller on stability and control characteristics, tests were made of a 0.32-scale model of a single-engine, fighter-type airplane in the NACA 19-foot pressure tunnel at Langley Field, Va. The investigation was confined to the determination of the characteristics in yaw with the vertical tail on and with the vertical tail off. The results of these tests are believed to be of no direct general application but serve as an indication of the character and magnitude of the effects of the two types of rotation.

APPARATUS AND TESTS

Model

The general dimensions of the model are given in figure 1. The wing was equipped with 0.25c partial-span slotted flaps and also with slats on the leading edge of the outer wing panels. Provision was made for air flow through the cowl, the two wing ducts, and the supercharger air duct located beneath the cowl. A detail drawing of the vertical tail surface is presented in figure 2. The vertical fin was set at 0° and the horizontal stabilizer at 2° for all tests.

The model was equipped with a six-blade propeller unit made up of two three-blade propellers having a distance between center lines of 4.05 inches. The blades were of the NACA 4-308-03 type; blade-form curves are presented in figure 3. In the dual-rotating unit, the front blades were right hand and the rear blades left hand. The propellers were driven through a dual-rotating gear box. In the single-rotating unit, the gear box was replaced by a solid coupling. Both the front and the rear blades were right hand and were equally spaced about the center of rotation. An electric motor capable of delivering a torque of 195 foot-pounds was used to drive the propeller unit.

Model configurations for landing and for normal flight were tested. In the landing configuration shown in figure 4, the wing flaps were deflected 50° , the ailerons were drooped 15° , the slats were open, the cowl-exit flap was deflected 25° , the oil-cooler and inter-cooler exit flap was deflected 22° , and the landing gear was installed. In the normal-flight configuration shown in figure 5, all the aforementioned surfaces were in the neutral position and the landing gear was removed.

Tests

The model mounted in the test section of the tunnel is shown in figures 4 and 5. Measurements were made of the six-component forces and moments on the model and of the rudder hinge moments. Forces were measured directly by the wind-tunnel balance and moments were computed from force readings. Rudder hinge moments were measured by electrical resistance-type strain gages.

The model was yawed, at selected angles of attack, through a range of angles of yaw from -10° to 40° for the dual-rotation tests and from -30° to 30° for the single-rotation tests. The yaw range was limited to these values by the model support. All tests were made with the air in the tunnel at an absolute pressure of 35 pounds per square inch. The test Reynolds number was approximately 3,000,000, except for a few tests made at a Reynolds number of 4,200,000.

In the normal-flight configuration, the model was tested simulating full power with the thrust line at an angle of attack of -0.8° , corresponding to high-speed level flight, and at an angle of attack of 11.8° , corresponding to a full-power climb at 107 percent of the power-off stalling speed. These conditions are hereinafter referred to as the "high-speed condition" and the "climb condition", respectively. In the landing configuration, the model was tested simulating 55-percent full power at an angle of attack of 10° corresponding to flight at 107 percent of the power-off stalling speed. This model and power condition is hereinafter referred to as the "approach condition". For these three conditions, tests were made for a range of rudder deflections and with the vertical tail off. In addition, for each angle of attack, tests were made with the propeller operating at approximately zero thrust, simulating an engine-idling glide, and also with the propeller off; these tests were made with rudder neutral and with the vertical tail off.

The power conditions of the model tested simulated those of the design airplane. Full power represents 2250 brake horsepower at sea level and 55-percent full power represents 1300 brake horsepower at sea level. The axial component of the slipstream velocity, as measured by the thrust coefficient T_c , was taken as the criterion of similitude of the power conditions. The calculated thrust coefficients for the dual-rotation case are shown in figure 6. The rotational component of the slipstream as measured by the torque coefficient Q_c is believed to be adequately reproduced for these tests. The thrust and torque characteristics of the model propellers, as determined experimentally with the thrust line horizontal, are given in figures 7 and 8. For each model condition, the single-rotating and the dual-rotating propellers were operated at approximately the same thrust coefficient. The blade angle at $r/R = 0.75$ radius was 23° for all tests. The propeller rotational speed was held constant throughout the yaw range.

Coefficients and Symbols

The data are presented in the form of standard, nondimensional coefficients. The coefficients and symbols are defined as follows:

C_L	lift coefficient (L/qS)
C_{D_R}	resultant drag coefficient (D_R/qS)
C_Y	lateral-force coefficient (Y/qS)
C_m	pitching-moment coefficient ($M/q\bar{c}S$)
C_n	yawing-moment coefficient (N/qbS)
C_{H_r}	rudder hinge-moment coefficient ($H_r/qb_r\bar{c}_r^2$)
T_c	thrust disk-loading coefficient ($T/\rho V^2 D^2$)
Q_0	torque coefficient ($Q/\rho V^2 D^3$)

where

L	lift
D_R	resultant drag
Y	lateral force
M	pitching moment
N	yawing moment
H_r	rudder hinge moment
T	effective thrust
Q	motor torque
S	wing area, 38.4 square feet
b	wing span, 14.72 feet
\bar{c}	mean wing chord, 2.61 feet
b_r	rudder span

\bar{c}_r	root-mean-square chord of rudder
D	propeller diameter, 4.0 feet
q	free-stream dynamic pressure
V	free-stream velocity
ρ	mass density of air
and	
n	propeller rotational speed
β	blade angle at 0.75 radius
α_T	angle of attack of thrust line, degree
ψ	angle of yaw, degree
δ_r	rudder deflection, degree
δ_e	elevator deflection, degree
R	Reynolds number $\left(\frac{\rho V \bar{c}}{\mu}\right)$
μ	coefficient of viscosity
$b_r \bar{c}_r^2$	$= 0.785 \text{ feet}^3$

Angle of attack, drag, and pitching moment have been corrected for the effects of jet-boundary interference. Approximate corrections have been applied for the effects of the model support.

All forces and moments are referred to a system of axes with the origin at the center of gravity corresponding to that of the full-scale airplane. The X-axis is the intersection of the plane of symmetry of the model with a plane perpendicular to the plane of symmetry and parallel to the relative wind with the positive direction rearward. The Y-axis is perpendicular to the plane of symmetry with the positive direction to the right. The Z-axis is perpendicular to the X-axis and in the plane of symmetry, with the positive direction upward.

RESULTS AND DISCUSSION

The test data are presented as curves of lift, resultant-drag, lateral-force, yawing-moment, pitching-moment, and rudder hinge-moment coefficients plotted against angle of yaw. No rolling-moment curves are presented because of inconsistencies in the data and a wide dispersion of test points. Yaw characteristics for a range of rudder deflections are presented in figures 9 to 14 for the approach, the climb, and the high-speed conditions. Comparisons of the effects of rotation on the yaw characteristics with the vertical tail on (rudder neutral) and with the vertical tail off are presented in figures 15 to 23 for the approach, the climb, the high-speed, and the glide conditions. In each case, propeller-off data are given as a basis for comparison.

From figures 9 to 14, estimates have been made of the rudder-control characteristics of the design airplane in steady sideslips. These data are presented in figures 24, 25, and 26 as curves of rudder force and deflection for trim against angle of yaw. The yawing moment due to aileron deflection was neglected in all cases. The control forces were calculated with the assumption of a pedal movement of $\pm \frac{1}{4}$ inches for $\pm 20^\circ$ rudder throw and a wing loading of 36 pounds per square foot. Left rudder forces and deflections with dual rotation were estimated by assuming that the curves would be symmetrical about neutral rudder.

Most of the important directional stability and control characteristics for the three model conditions are summarized in table I. Slopes of the yawing-moment curves at zero yaw for the various model conditions are given in table II.

All data are presented for zero fin offset and neutral trim-tab setting. A small fin offset with single rotation would probably not appreciably alter the general conclusions. The comparisons made with the rudder trim tab neutral are not entirely complete because a tab would ordinarily be deflected with single rotation in some of the flight conditions. The deflected tab would affect, to some extent, almost all directional stability and control characteristics. It should be noted that the knife-edge shape of the rear end of the fuselage provides appreciable fin area even with the vertical tail off.

Inasmuch as the thrust coefficient and the angle of attack are nearly the same for the approach and the climb conditions, these two conditions differ principally in that the climb is a flaps-up condition and the approach is a flaps-down condition. Although the two model configurations differ in more respects than this one, the differences in yaw characteristics are believed to be due primarily to flap deflection.

The discussion of the data is devoted almost entirely to static directional stability and control. Although rolling-moment data are not presented, it should be remembered that there are large lateral-trim changes requiring the use of ailerons in the high-thrust conditions with single-rotating propellers. In the comparison of the results for dual rotation with those for single rotation, the assumption was made that with dual rotation the curves for left rudder deflections would be similar to those for right rudder deflections.

The data show that for the high-thrust conditions, where the slipstream effects are large, the yaw characteristics are asymmetrical about zero yaw with single rotation and are essentially symmetrical with dual rotation. For the low-thrust conditions, the yaw characteristics were nearly symmetrical about zero yaw for both single and dual rotation.

Directional trim change.- In the low-speed high-thrust conditions, directional trim changes are negligible with dual rotation and large with single rotation. With dual rotation, zero yaw can be maintained with approximately neutral rudder and zero control force in both the climb and approach conditions (figs. 24 and 25). With single rotation, a right rudder deflection of 18° is required to hold zero yaw; the estimated rudder forces are 125 pounds and 70 pounds for the climb and the approach conditions, respectively. The maximum rudder deflection of 20° would not be sufficient to trim the airplane at the angle of yaw necessary for straight flight with wings level ($\psi = 5^\circ$). This angle of yaw is taken as the angle at which both the lateral force and the yawing moment are zero if the yawing moment due to aileron deflection is neglected. For dual rotation in all conditions and for single rotation in the high-speed condition, the wings can be kept level at zero yaw and little rudder deflection is needed.

With single rotation and rudder neutral, the model trims ($C_n = 0$) at an angle of yaw of about -10° . At zero yaw, there is a large negative yawing moment as shown in figures 15 and 17. At least half of this moment is contributed by the model without the vertical tail. (See figs. 16 and 18.)

Directional stability, rudder-fixed.- In the high-thrust conditions, the displacement of the single-rotation yawing-moment curves toward negative C_n and negative ψ , resulted in a tendency toward directional instability at moderate to large negative angles of yaw. With single rotation, instability is indicated in the approach condition at an angle of yaw of -27° with full left rudder ($\delta_r = 20^\circ$). In the climb condition positive stability is shown in the trim range; however, the slope of the yawing-moment curve tends to become unstable at about $\psi = -30^\circ$ for conditions only slightly out of trim. With dual rotation, stability is indicated in the trim range for both the climb and the approach conditions. Beyond the trim range, reversals of the yawing-moment-curve slopes occur in the approach (flaps-down) condition but not in the climb (flaps-up) condition. The reversals in the approach condition might lead to directional instability if the rudder limit were increased to about 30° . For a greater rudder range, the directional instability with single rotation would be aggravated. It would be desirable, in this case, to restrict the left rudder range and increase the right rudder range.

Up to moderate angles of negative yaw, the stability was greater with single rotation than with dual rotation, except for the glide conditions (propeller at zero thrust) where little difference was shown. At zero yaw in the approach, climb, and high-speed conditions, the moment-curve slopes were about 15 percent more stable with single rotation than with dual rotation. In the approach condition (figs. 9 and 10), this difference was essentially constant up to $\psi = -15^\circ$ (dual-rotation curves are assumed symmetrical), but for the climb condition (figs. 11 and 12) considerably steeper slopes were obtained with single rotation in the region of $\psi = -10^\circ$. The aforementioned differences in stability should not be important except in marginal cases.

The more stable moment-curve slopes with single rotation in the approach and the climb conditions appear to be due partly to the more stable slopes for the model without the vertical tail and partly to the greater effect of the vertical tail.

In the high-speed condition (figs. 19 and 20), where the lift coefficient and thrust coefficient are low, the decrease in stability with dual rotation would appear to be due primarily to the increase in propeller side force experienced with a dual-rotating propeller (references 2 and 3). In figure 27 the measured yawing moments due to the propeller ($C_{n\text{propeller on}} - C_{n\text{propeller off}}$) obtained from figure 20 are compared with the yawing moments calculated by use of the theoretical propeller side forces determined from the charts of reference 2. The comparison indicates that the differences in the yawing moments caused by a single-rotating and by a dual-rotating propeller were somewhat greater from experiment than from calculation. In addition, measured yawing moments due to either type of propeller were greater than corresponding calculated yawing moments. Measured side forces due to the propeller, however, are lower than the theoretical propeller side forces. It is concluded, therefore, that the effects of the propeller were not restricted to direct propeller forces but included forces on the airplane itself, which affected the over-all side force and yawing moment.

Directional stability, rudder free.- Rudder-free (pedal-free) yawing moments, obtained by cross-plotting, are shown in figures 9 to 12. In the approach condition, the yawing moment is stable with dual rotation but unstable beyond $\psi = -25^\circ$ with single rotation. The instability with single rotation occurred in a manner termed "rudder lock"; that is, as the increasingly unstable yawing moment yaws the airplane to the left, the hinge moment forces the rudder continually harder against the stop. In the climb condition, the rudder-free moment is restoring except at $\psi = -24^\circ$ with single rotation and at $\psi = \pm 23^\circ$ with dual rotation where the moments are zero. The rudder limit is particularly critical to the rudder-free stability at large angles of yaw and the stability would be unfavorably affected by a greater rudder range in all conditions.

Rudder-control effectiveness.- In the high-speed and approach conditions (figs. 24 and 26), the rudder-control effectiveness $d\psi/d\delta_r$ was about 10 percent greater with dual rotation than with single rotation over the straight portions of the curves. In the climb condition, the average effectiveness with dual rotation was about twice that with single rotation. This increase in effectiveness is a result of the lower weathercock stability with dual rotation. In the climb condition, the angles of yaw maintained by $\pm 20^\circ$ rudder deflection were $\pm 21^\circ$ with dual rotation and were 2° and -23° with single rotation. In the approach condition angles of yaw maintained by maximum rudder deflections were $\pm 11^\circ$ for dual rotation and were 2° and -23° for single rotation.

Rudder-control forces.- As mentioned previously, the calculated rudder forces required to trim at zero yaw with single rotation are 125 pounds for the climb and 70 pounds for the approach condition; with dual rotation the rudder forces are approximately zero.

The control forces per degree of yaw in the approach and climb conditions are two to three times greater with single rotation than with dual rotation in the straight-line portion of the curves (figs. 24 and 25). In the high-speed condition (fig. 26), the force gradients were the same. The displacement of the rudder-force curves in figure 26 should not be considered significant because a small error in rudder-angle or hinge-moment measurement would be greatly magnified in the force curves.

At large angles of yaw, the forces either are zero or change sign with single rotation in the approach and climb conditions and with dual rotation in the climb condition. A rudder range greater than $\pm 20^\circ$ would accentuate these force reversals and might cause a reversal in the approach condition with dual rotation if the travel were increased sufficiently. Since the trim requirements are less severe with dual than with single rotation, it appears that increased travel would not be required with dual rotation.

Inasmuch as a tab would normally be used with single-rotating propellers to trim out control forces at zero yaw, the variations of force with angle of yaw for the approach and climb conditions would probably be different from those indicated in figures 24 to 26.

Miscellaneous characteristics.- In the low-thrust conditions, only small differences between single and dual rotation were shown in lift, drag, pitching moment, and lateral force. In the high-thrust conditions, these characteristics were asymmetrical about zero yaw with single rotation and essentially symmetrical with dual rotation.

CONCLUSIONS

The results presented lead to the following conclusions with regard to the yaw characteristics of the single-engine airplane model with a single-rotating and a dual-rotating propeller:

1. The most noticeable differences shown were the large directional trim changes with the single-rotating propeller and the negligible trim changes with the dual-rotating propeller. With single rotation large rudder deflections and forces were required to trim ($C_n = 0$) at zero yaw in the low-speed high-thrust conditions, whereas with dual rotation only small deflections and forces were required.
2. The model with dual-rotating propeller was directionally stable with rudder fixed throughout the trim range for all conditions. Beyond the trim range, reversals of the yawing-moment curves occurred in the approach condition; these reversals might produce instability if the rudder range were increased sufficiently. With single rotation, rudder fixed, the model was unstable at large angles of left yaw in the approach (flaps-down) condition and exhibited a tendency to be unstable in the climb (flaps-up) condition. The instability in the approach condition also occurred with rudder free and in a manner termed "rudder lock"; that is, as the increasingly unstable yawing moment yaws the airplane to the left, the hinge moment forces the rudder continually harder against the stop.
3. Although of secondary importance for the model tested, a greater degree of rudder-fixed stability was generally shown with single rotation than with dual rotation at small to moderate angles of yaw. At zero yaw, the slopes of the yawing-moment curves were about 15 percent more stable with single rotation in the approach, climb, and high-speed conditions than with dual rotation.

4. The rudder-control effectiveness $dW/d\delta_r$ in the high-speed condition was about 10-percent greater with dual rotation than with single rotation. In the climb condition, angles of yaw maintained by $\pm 20^\circ$ rudder were $\pm 21^\circ$ with dual rotation, and 2° and -23° with single rotation. In the approach condition, the angles of yaw were $\pm 11^\circ$ with dual rotation, and 2° and -23° with single rotation.

5. The rudder-control forces per degree of yaw were two to three times as great for single rotation as for dual rotation in the low-speed high-thrust conditions.

Langley Memorial Aeronautical Laboratory,
National Advisory Committee for Aeronautics.
Langley Field, Va.

REFERENCES

1. Sweberg, Harold H.: Air-Flow Surveys in the Region of the Tail Surfaces of a Single-Engine Airplane Equipped with Dual-Rotating Propellers. NACA ACR, March 1943.
2. Ribner, Herbert S.: Formulas for Propellers in Yaw and Charts of the Side-Force Derivative. NACA ARR No. 3E19, 1943.
3. Runckel, Jack F.: The Effect of Pitch on Force and Moment Characteristics of Full-Scale Propellers of Five Solidities. NACA ARR, June 1942.

TABLE I

COMPARISON OF ESTIMATED DIRECTIONAL STABILITY AND CONTROL CHARACTERISTICS
OF THE SINGLE-ENGINE AIRPLANE WITH A SINGLE-ROTATING
AND WITH A DUAL-ROTATING PROPELLER

[For conditions of $C_n = 0$; C_n due to aileron deflection is neglected].

Type of Rotation	δ_r at $\psi = 0^\circ$ (deg)	Rudder force at $\psi = 0^\circ$ (lb)	ψ at $\delta_r = 0^\circ$ (deg)	ψ for wings level, C_n and $C_y = 0$ (deg)	ψ at $\delta_r = \pm 20^\circ$ (deg)	Relative rudder effectiveness based on $\frac{d\psi}{d\delta_r}$ (percent) (a)	Relative rudder force per deg yaw (percent) (a)	Relative rudder-fixed stability based on $\frac{dC_n}{d\psi}$ (percent) (a)	ψ at which rudder-fixed instability occurs (deg)	ψ at which rudder-force reversal occurs (deg)
High-speed condition; $T_0 = 0.03$										
Single	0	25 (right)	0	0	± 14 (est.)	90	100	115	None indicated	None indicated
Dual	1 (left)	0	1	0	± 15 (est.)	100	100	100	--Do--	Do.
Full-power climb; flaps up; $T_0 = 0.55$										
Single	-18 (right)	125 (right)	-12	^b 6	2, -23	60	300	115	Possibly beyond -30	-23
Dual	1 (left)	10 (right)	1	0	± 21	100	100	100	None indicated	± 20 (approx.)
Partial-power approach; flaps down; $T_0 = 0.59$										
Single	-17 (right)	70 (right)	-9	^b 4	2, -23	90	300	120	-26	-22
Dual	0	5 (right)	0	0	± 11	100	100	100	None indicated	None indicated

^aFor small angles of yaw

^bBeyond rudder control range

TABLE II
SLOPES OF YAWING-MOMENT CURVES AT ZERO YAW

Propeller condition	$dC_n/d\psi$				
	Normal flight			Landing	
	$\alpha_T = -0.8^\circ$	$\alpha_T = 11.8^\circ$	$\alpha_T = 11.8^\circ$	$\alpha_T = 10^\circ$	$\alpha_T = 9.8^\circ$
	High-speed level flight	Full-power climb	Propeller idling	Partial-power approach	Propeller idling
Vertical tail on ¹					
Propeller off	-0.0022	-0.0019	-0.0019	-0.0027	-0.0027
Single rotation	-.0015	-.0028	-.0012	-.0035	-.0018
Dual rotation	-.0013	-.0024	-.0009	-.0030	-.0018
Vertical tail off					
Propeller off	-0.0002	0.0001	0.0001	-0.0006	-0.0006
Single rotation	.0002	.0006	-----	-.0006	.0001
Dual rotation	.0005	.0006	-----	-.0005	0

¹Slopes are given for $C_n = 0$, rudder fixed

INDEX TO FIGURES

Figure	Information in figure				
1	Three-view drawing of model				
2	Details of vertical tail				
3	Propeller blade-form curves				
4	Model mounted in tunnel, landing configuration				
5	Model mounted in tunnel, normal-flight configuration				
6	Variation of thrust coefficient with lift coefficient				
7	Characteristics of dual-rotating propeller				
8	Characteristics of single-rotating propeller				
	Data presented	Flight condition	Model configuration	Rotation	Remarks
9	Yaw characteristics	Approach	Landing	Single	δ_r range
10	Do.-----	---do.---	--do.---	Dual	--do.---
11	Do.-----	Climb	Normal-flight	Single	--do.---
12	Do.-----	---do.---	--do.---	Dual	--do.---
13	Do.-----	High-speed	--do.---	Single	--do.---
14	Do.-----	---do.---	--do.---	Dual	--do.---
15	Effect of rotation on yaw characteristics	Approach	Landing	-----	$\delta_r = 0^\circ$
16	Do.-----	---do.---	--do.---	-----	Tail off
17	Do.-----	Climb	Normal-flight	-----	$\delta_r = 0^\circ$
18	Do.-----	---do.---	--do.---	-----	Tail off
19	Do.-----	High-speed	--do.---	-----	$\delta_r = 0^\circ$
20	Do.-----	---do.---	--do.---	-----	Tail off
21	Do.-----	Power-off glide	--do.---	-----	$\delta_r = 0^\circ$
22	Do.-----	---do.---	Landing	-----	$\delta_r = 0^\circ$
23	Do.-----	---do.---	--do.---	-----	Tail off
24	Steady sideslip characteristics, approach condition				
25	Steady sideslip characteristics, climb condition				
26	Steady sideslip characteristics, high-speed condition				
27	Comparison of experimental and calculated yawing moments due to propeller				

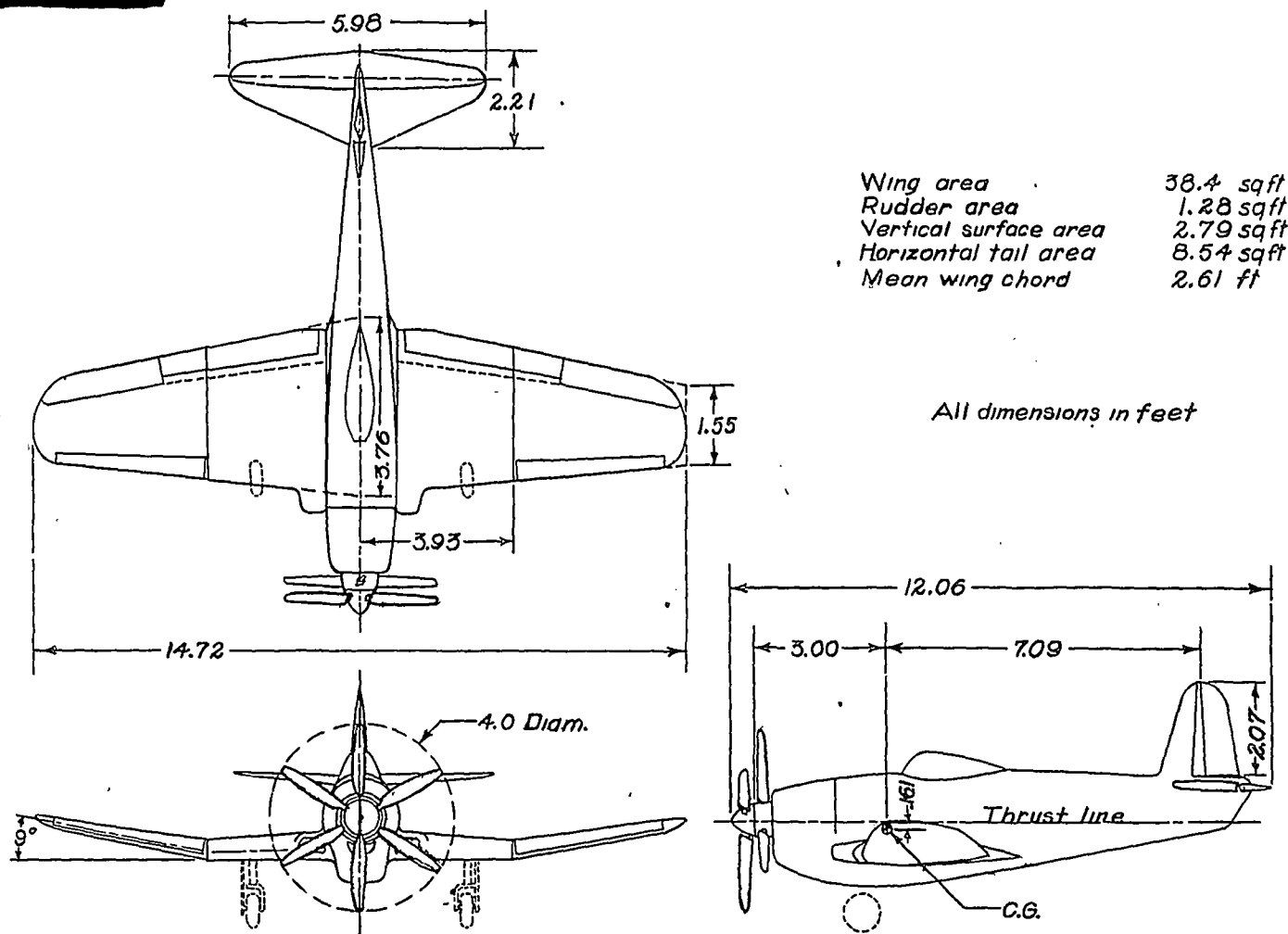
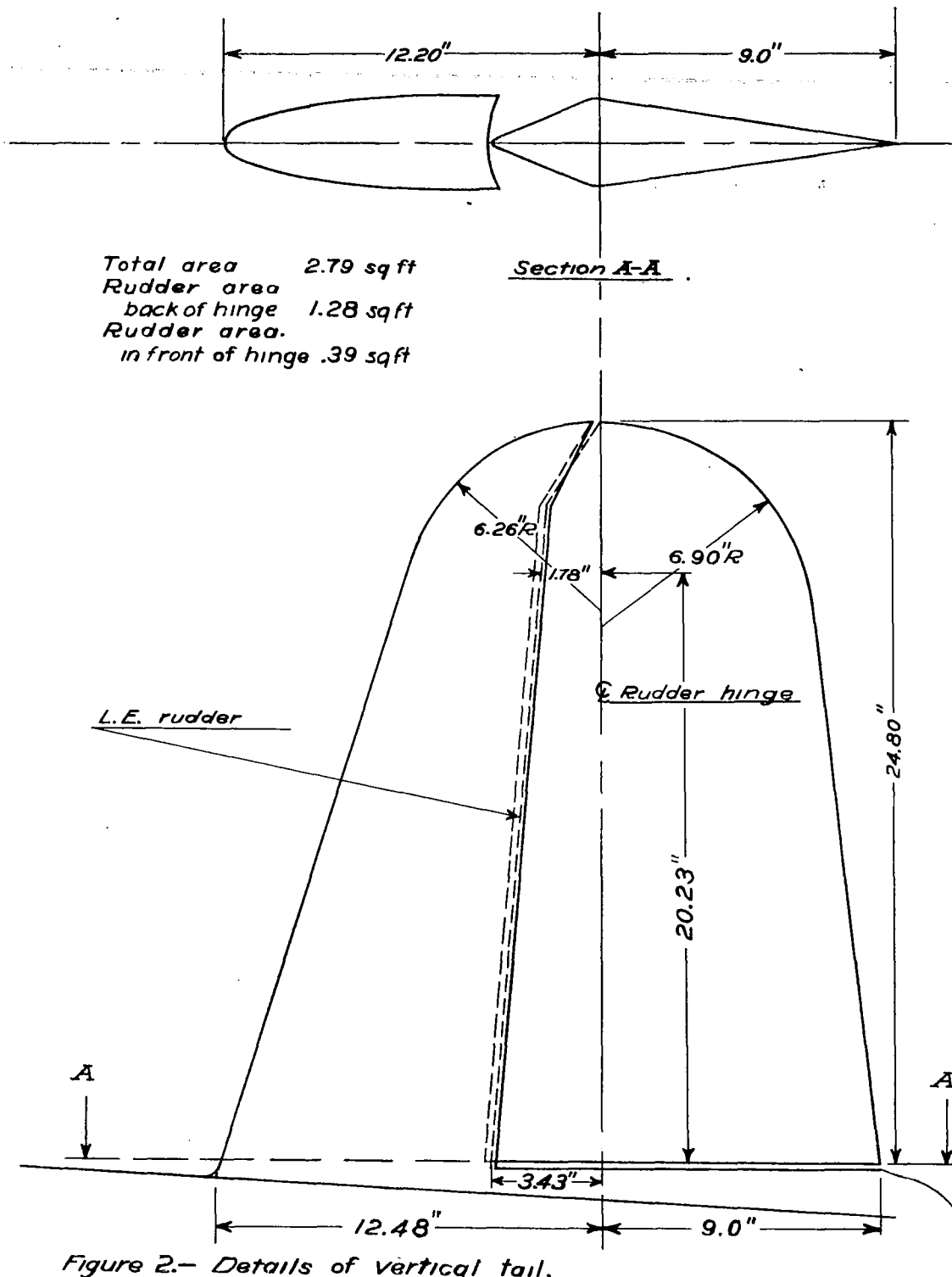


Figure 1.—Three-view drawing of model.



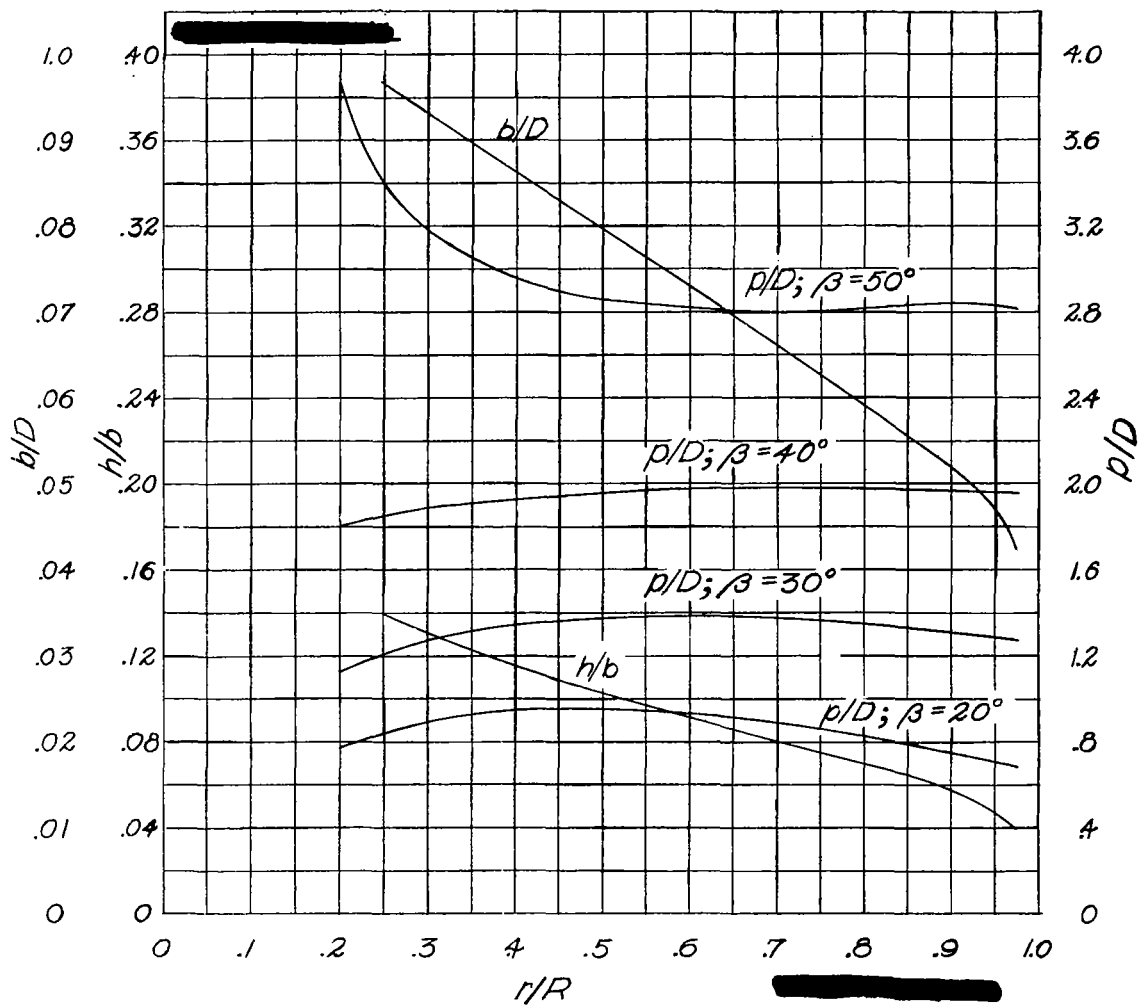


Figure 3. - Blade-form curves for NACA 4-308-03 propeller. D , diameter; R , radius to tip; r , station radius; b , section chord; h , section thickness; p , geometric pitch.

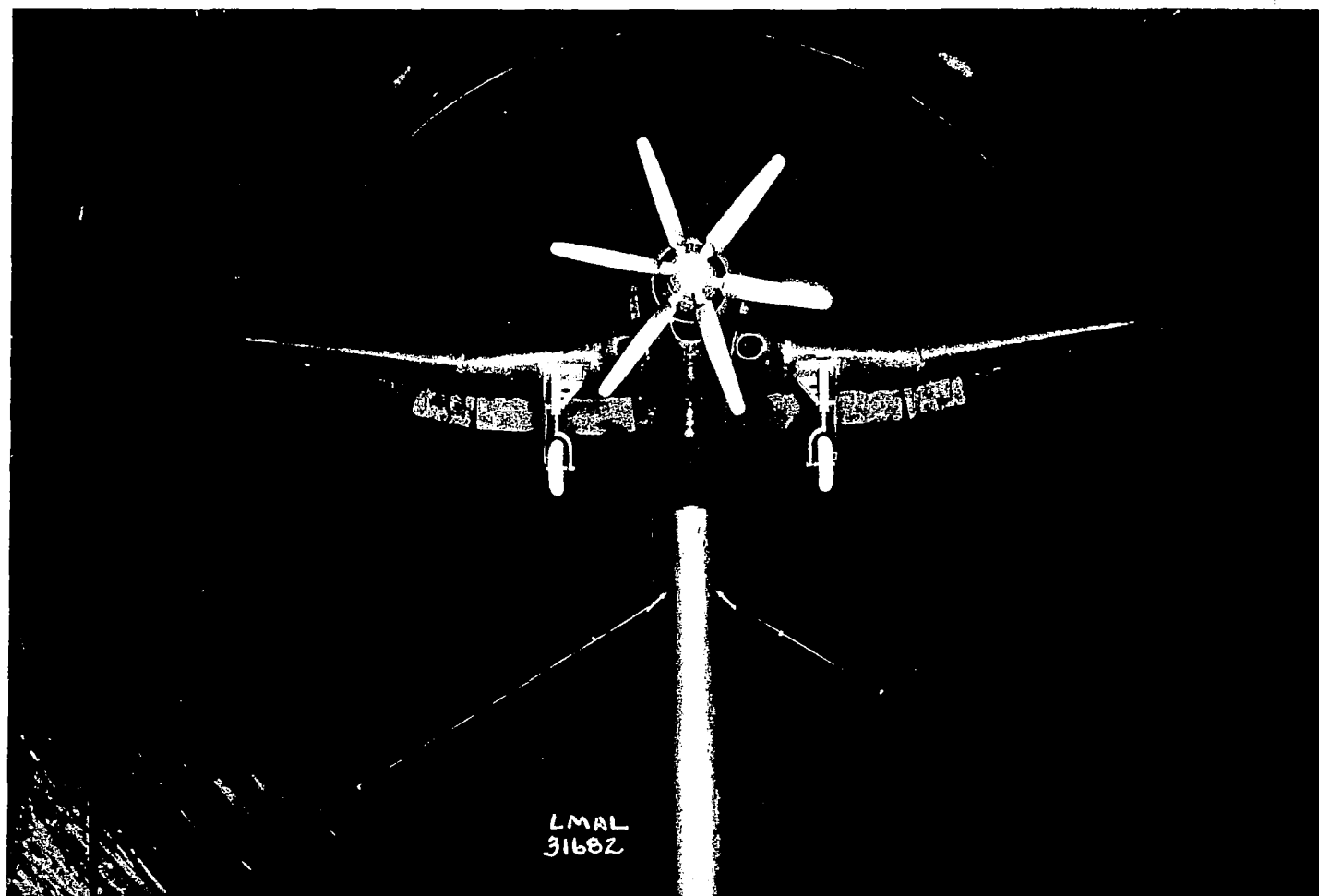


Figure 4.- Model mounted in NACA 19-foot pressure tunnel.
Landing configuration.

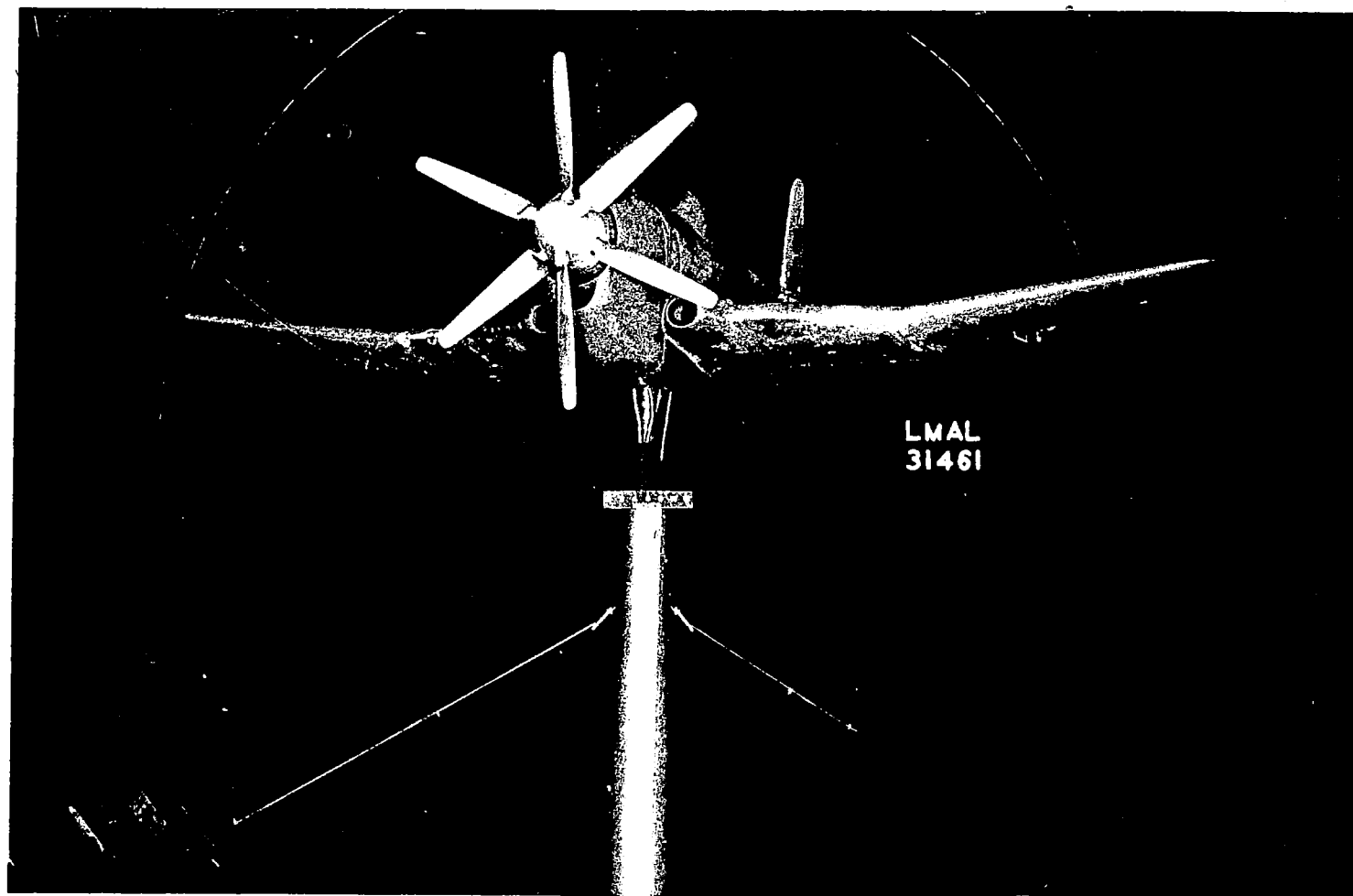


Figure 5.- Model mounted in NACA 19-foot pressure tunnel.
Normal-flight configuration.

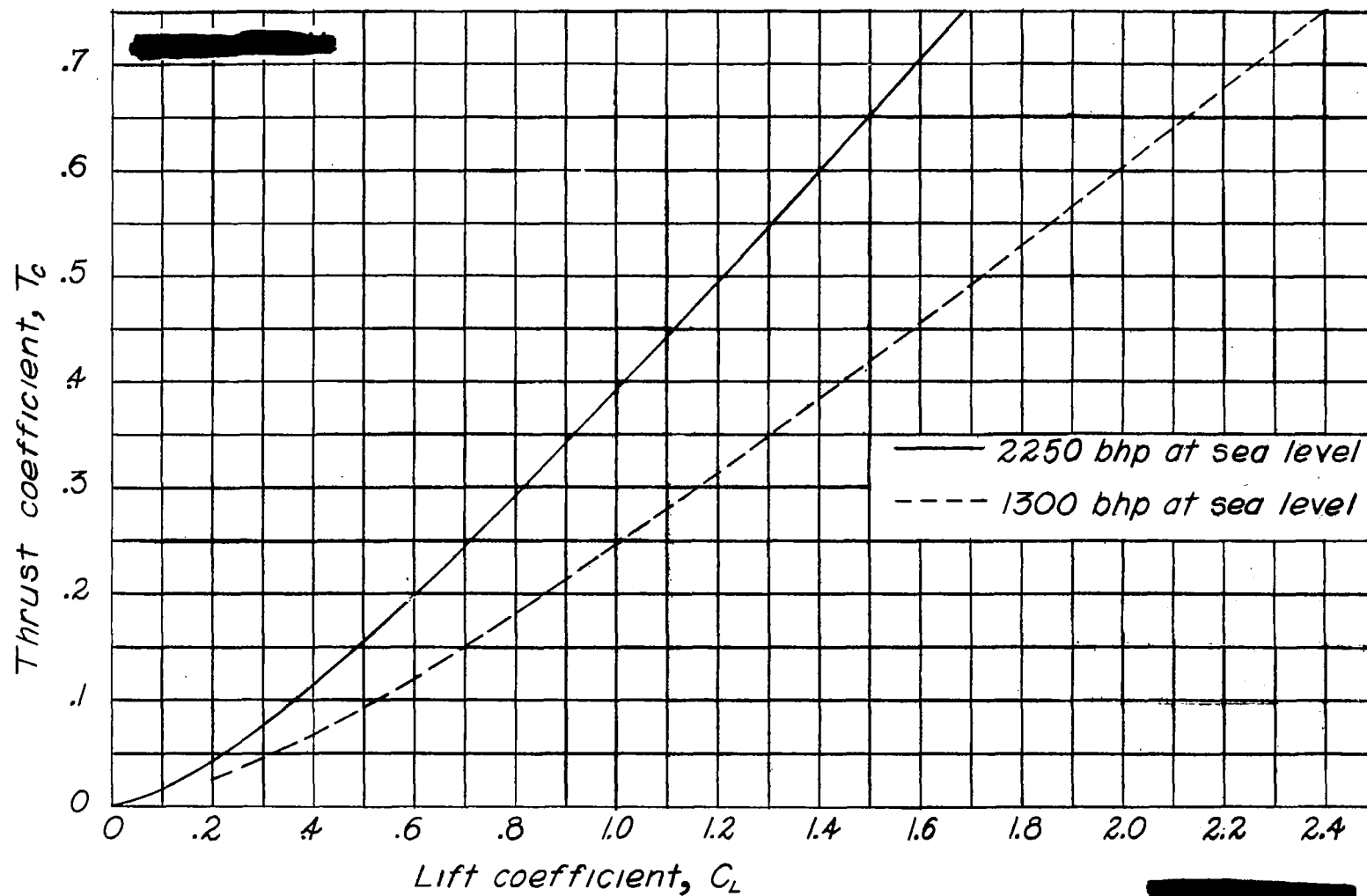


Figure 6.— Calculated full-scale thrust coefficients with dual rotation.

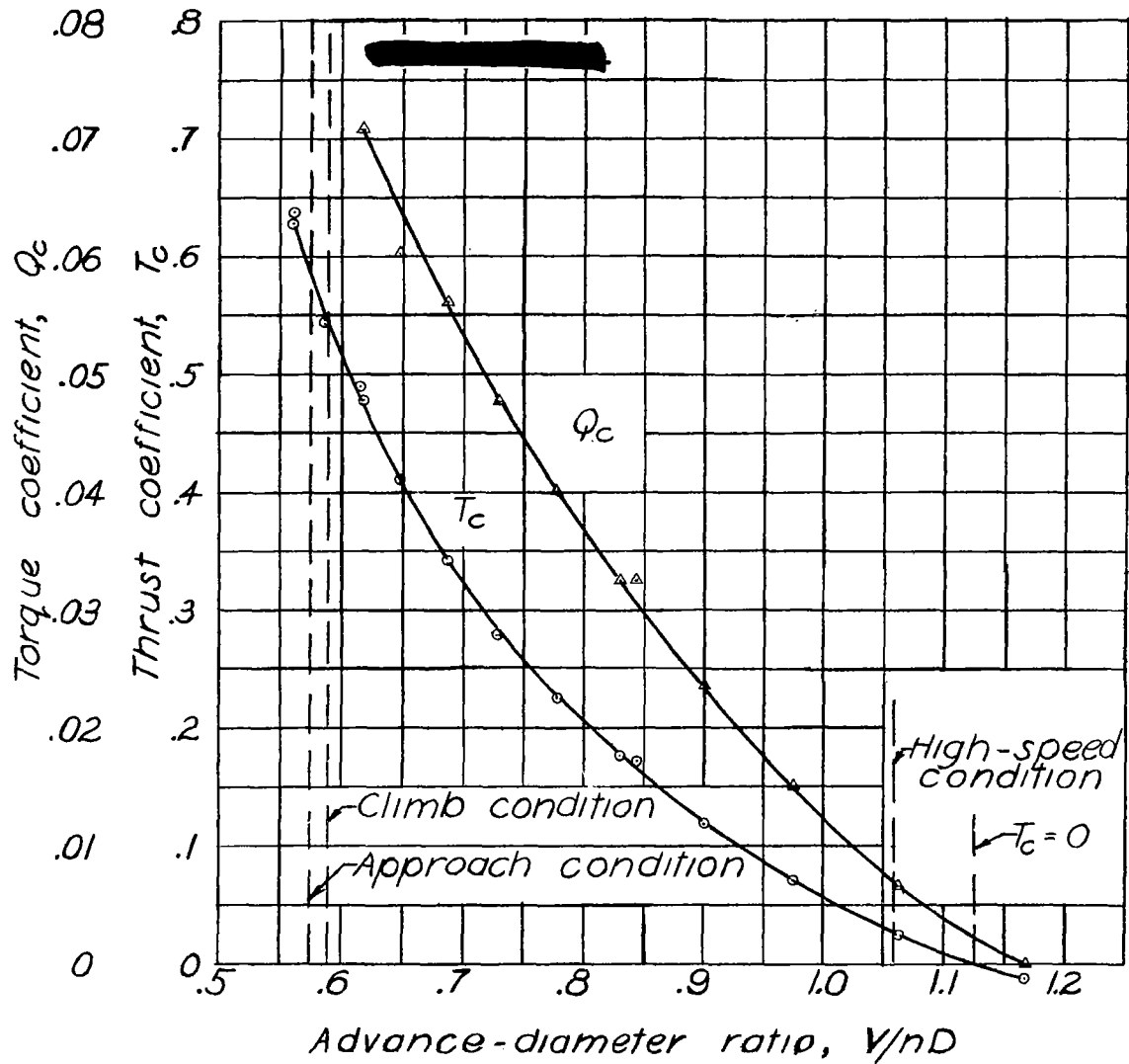


Figure 7.- Characteristics of the six-blade dual-rotating propeller; NACA 4-308-03 blades; $\beta = 23^\circ$; $D = 4$ feet.

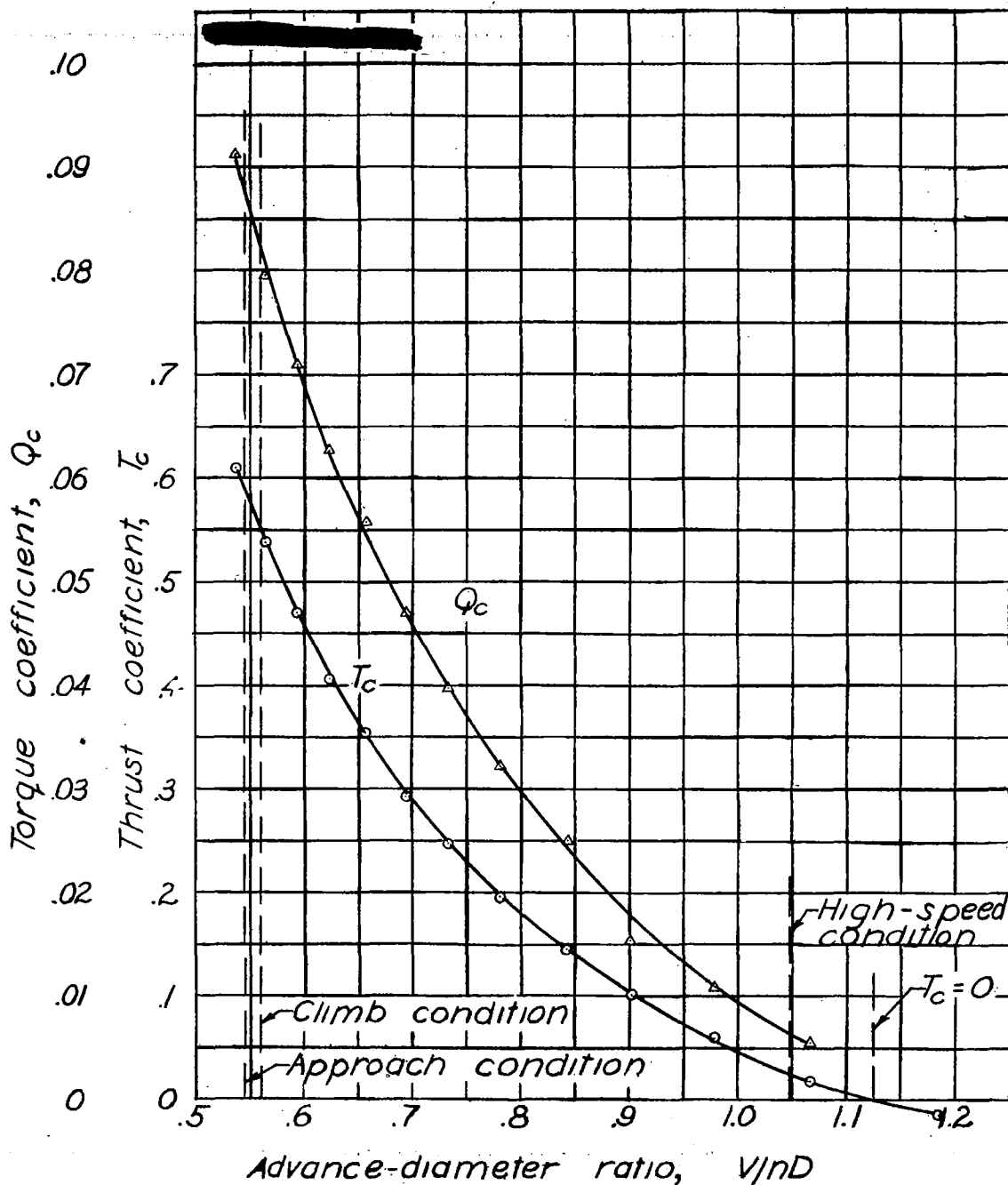


Figure 8.- Characteristics of the six-blade single-rotating propeller; NACA 4-308-03 blades; $\beta = 23^\circ$; $D = 4$ feet.

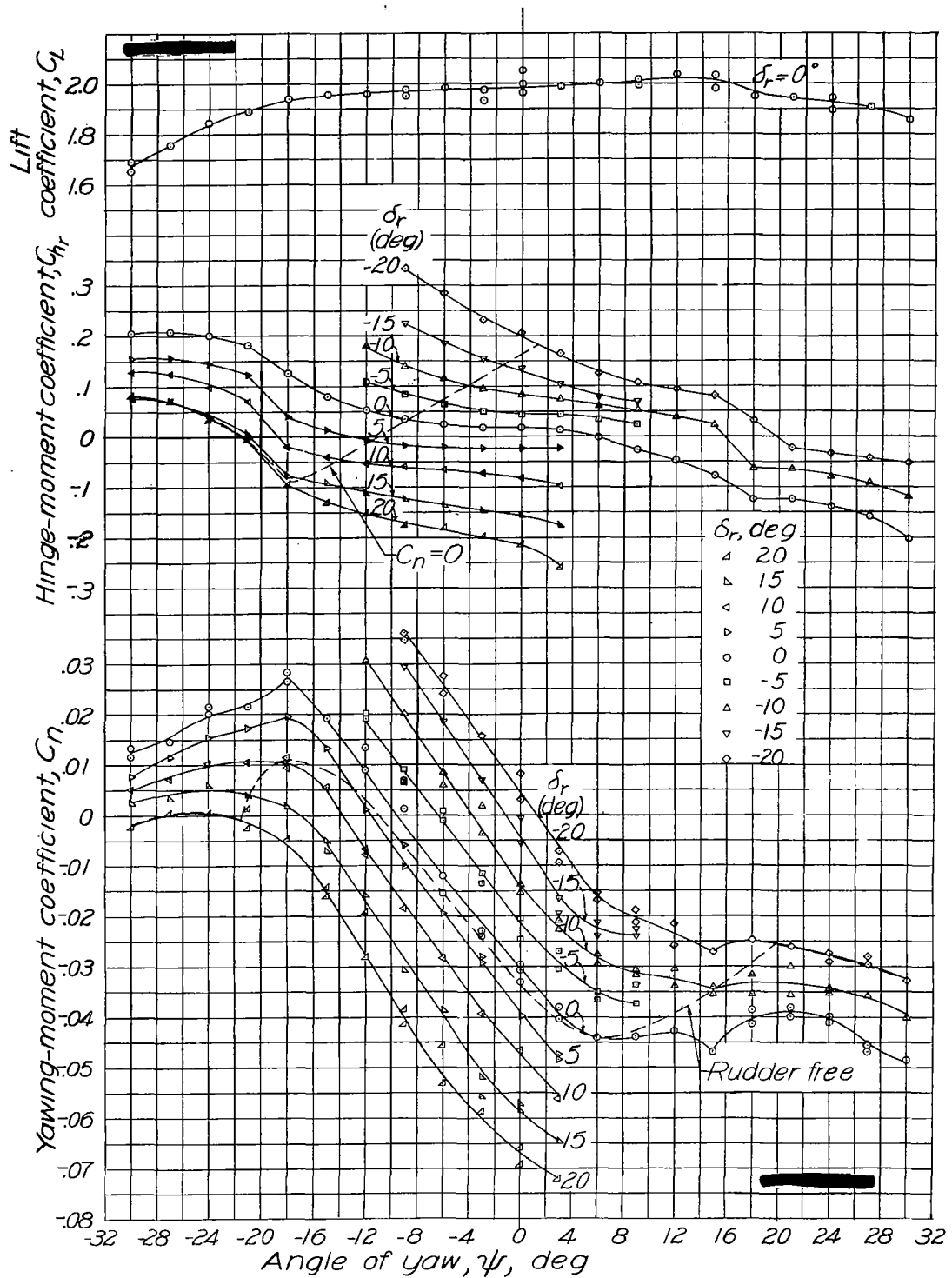


Figure 9.- Yaw characteristics for the approach condition. Single rotation; landing configuration; 55-percent full power; $T_c = 0.59$; $\alpha_T = 10^\circ$; $\delta_e = -3^\circ$; $R \approx 3,000,000$.

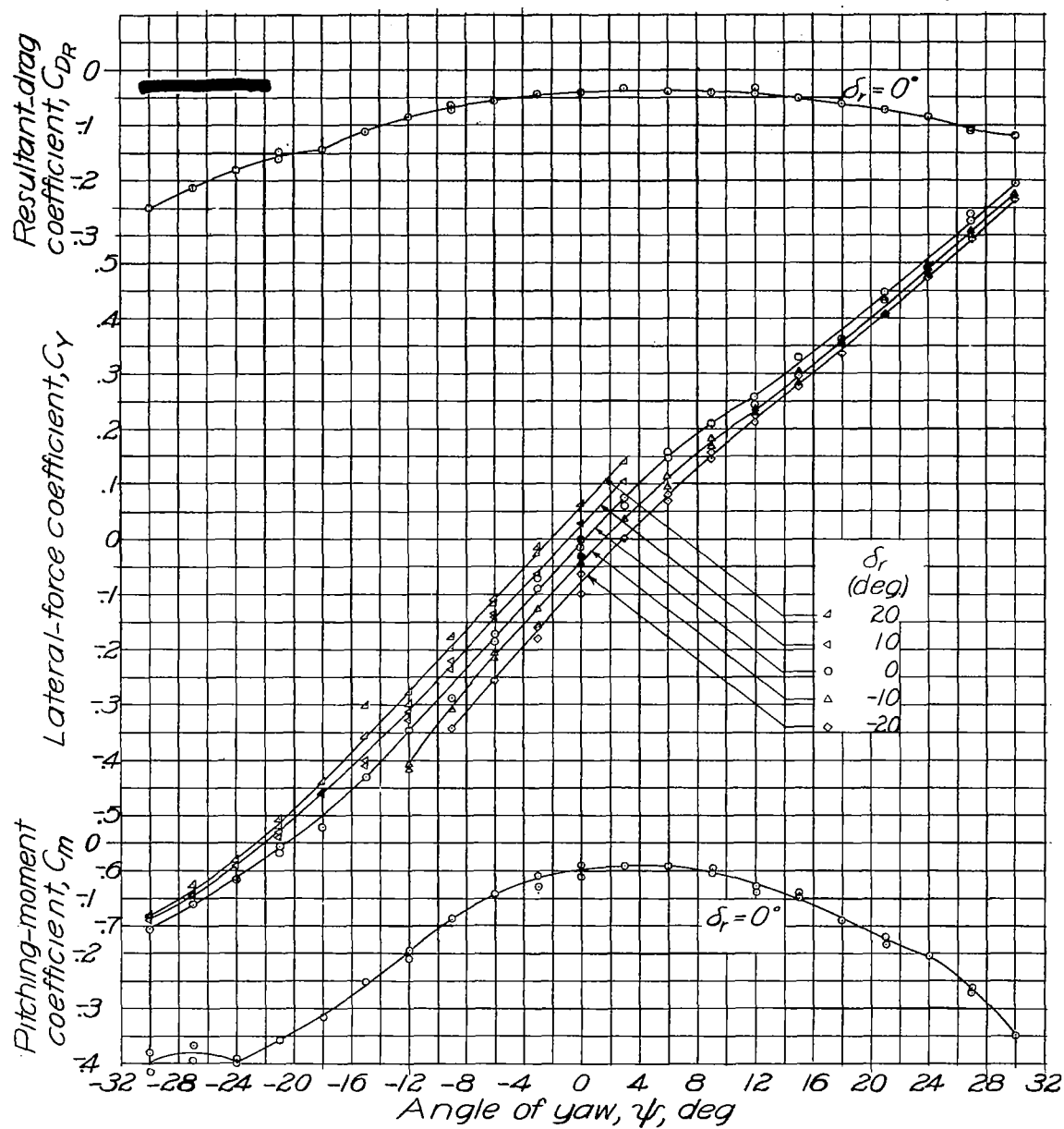


Figure 9.- Concluded.

Fig. 10a

NACA ACR No. L4D19

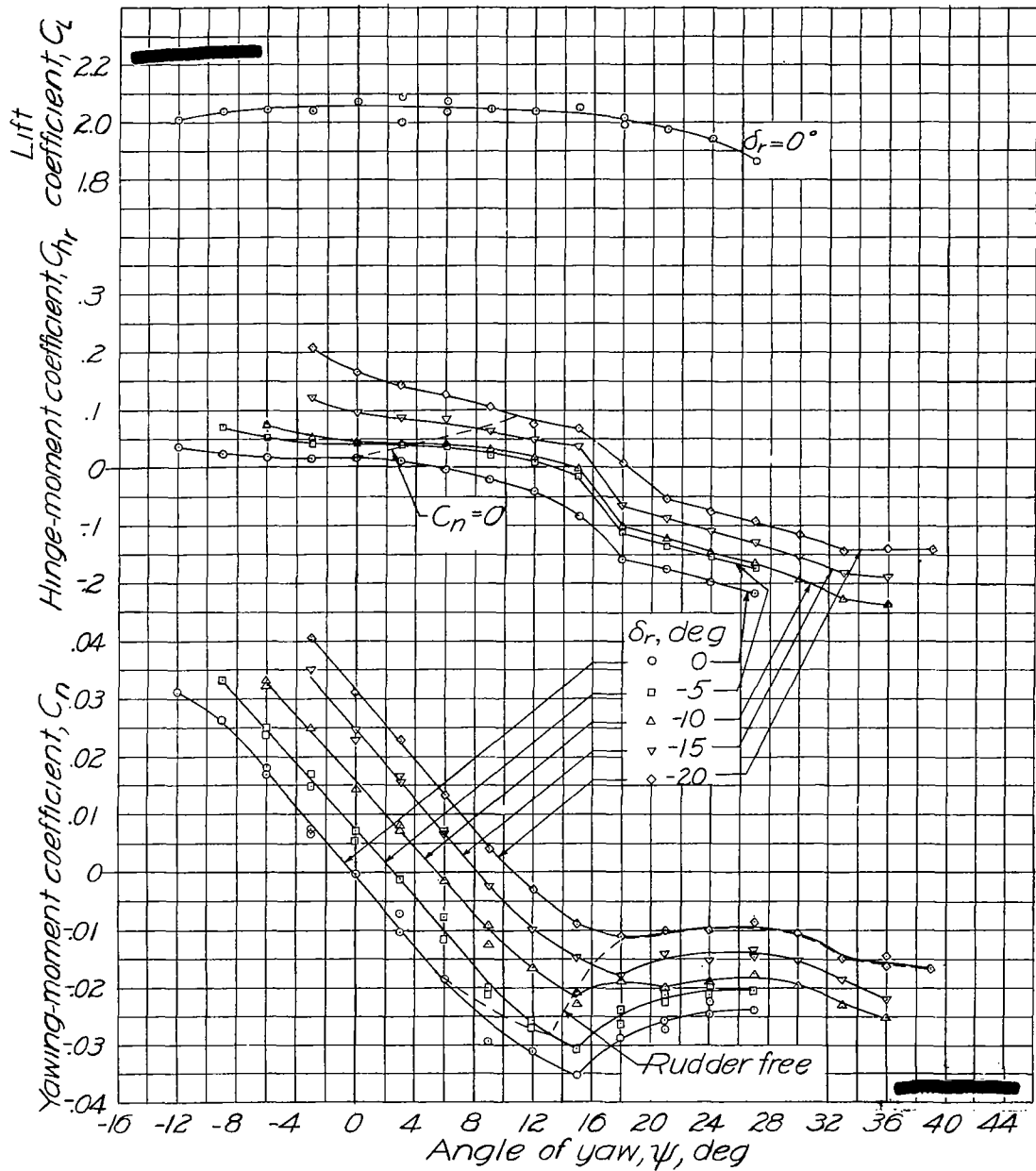


Figure 10.-Yaw characteristics for the approach condition. Dual rotation; landing configuration; 55-percent full power; $T_c = 0.59$; $\alpha_T = 10^\circ$; $\delta_e = -3^\circ$; $R \approx 3,000,000$.

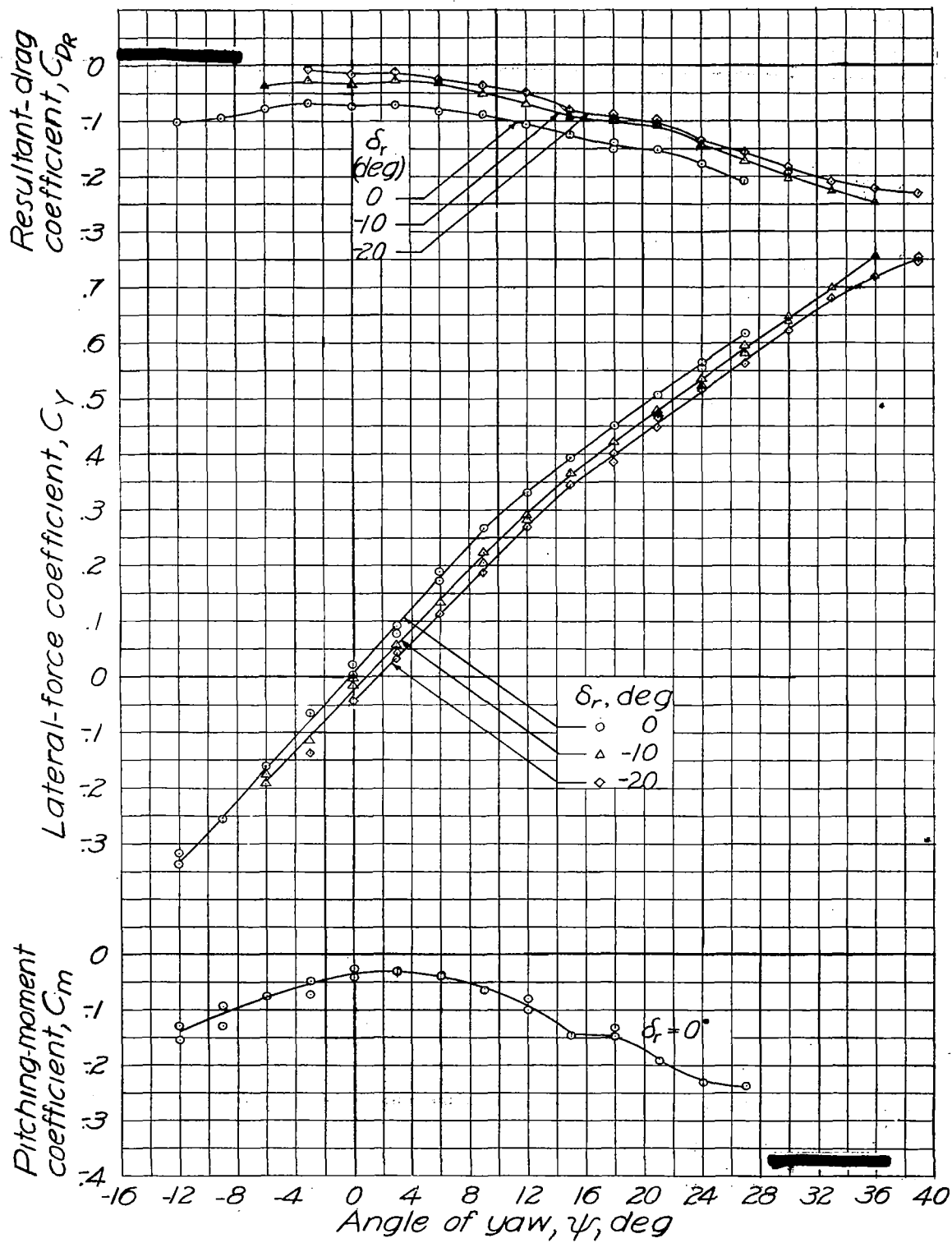


Figure 10.- Concluded.

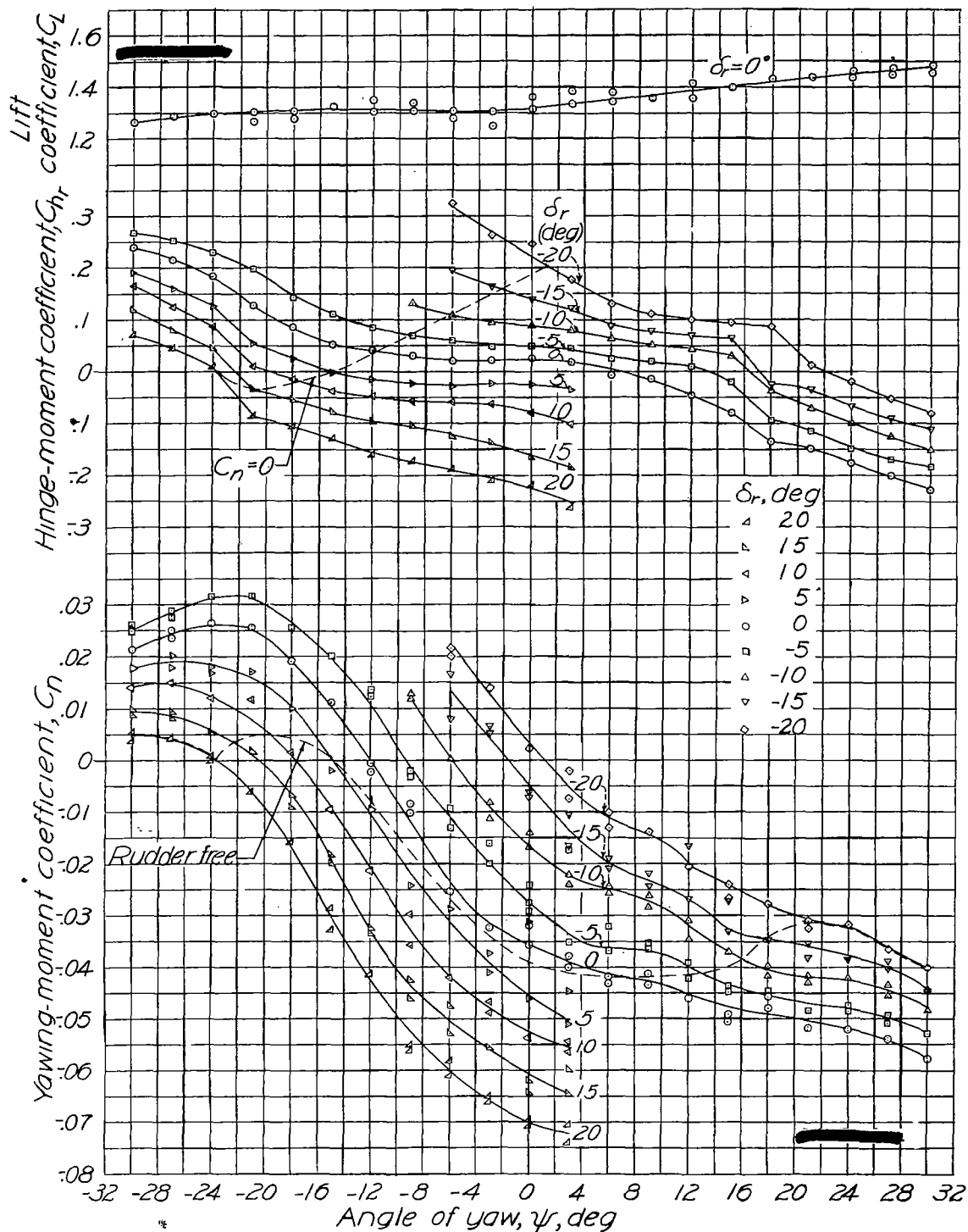


Figure 11.-Yaw characteristics for the climb condition. Single rotation; normal-flight configuration, full power, $T_c=0.55$; $\alpha_T=11.8^\circ$; $\delta_e=0^\circ$; $R \approx 3,000,000$.

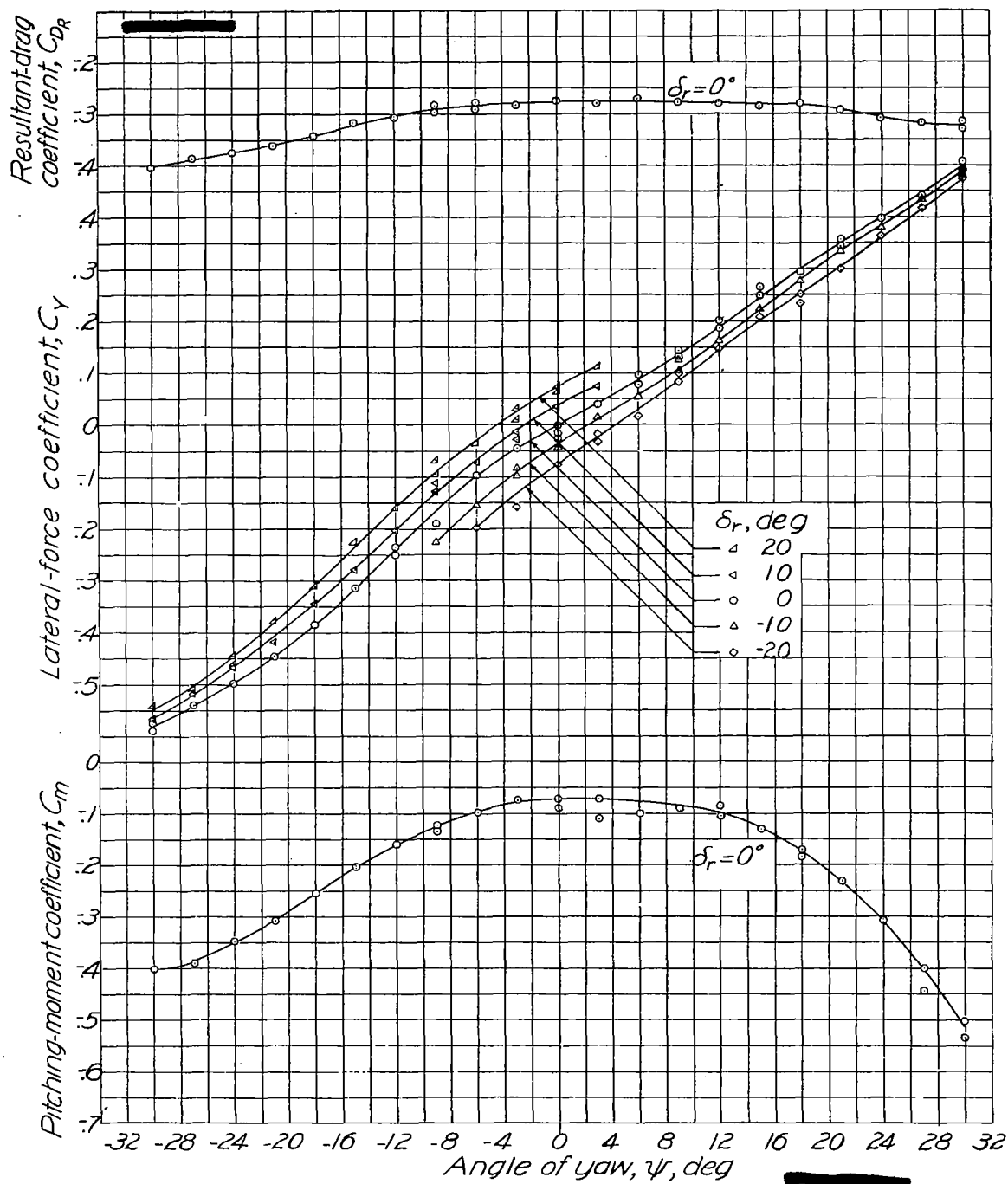


Figure 11.- Concluded.

Fig. 12a

NACA ACR No. L4D19

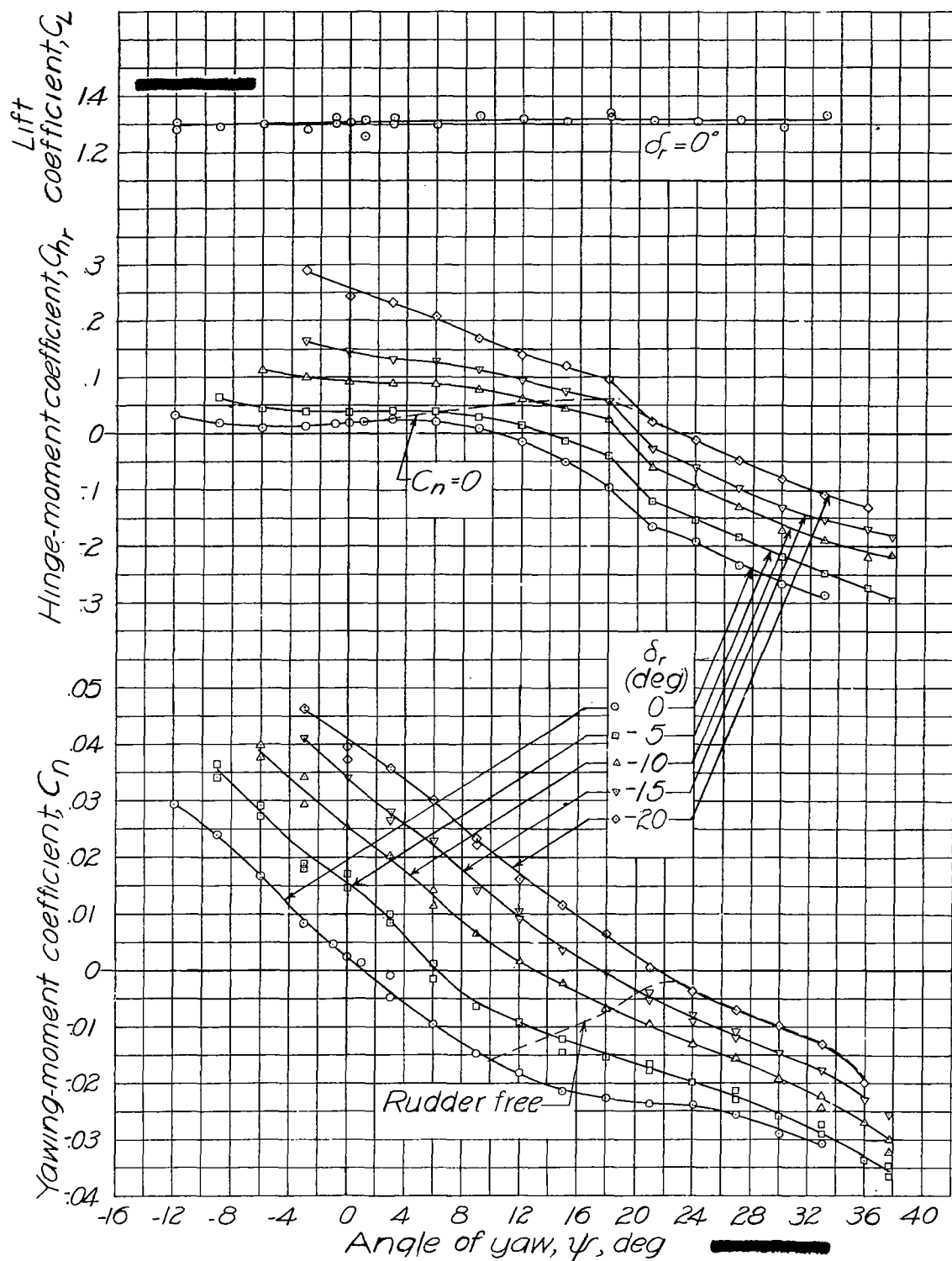


Figure 12.- Yaw characteristics for the climb condition. Dual rotation; normal-flight configuration; full power; $T_c = 0.55$; $\alpha_r = 11.8^\circ$; $\delta_e = 0^\circ$; $R = 3,000,000$.

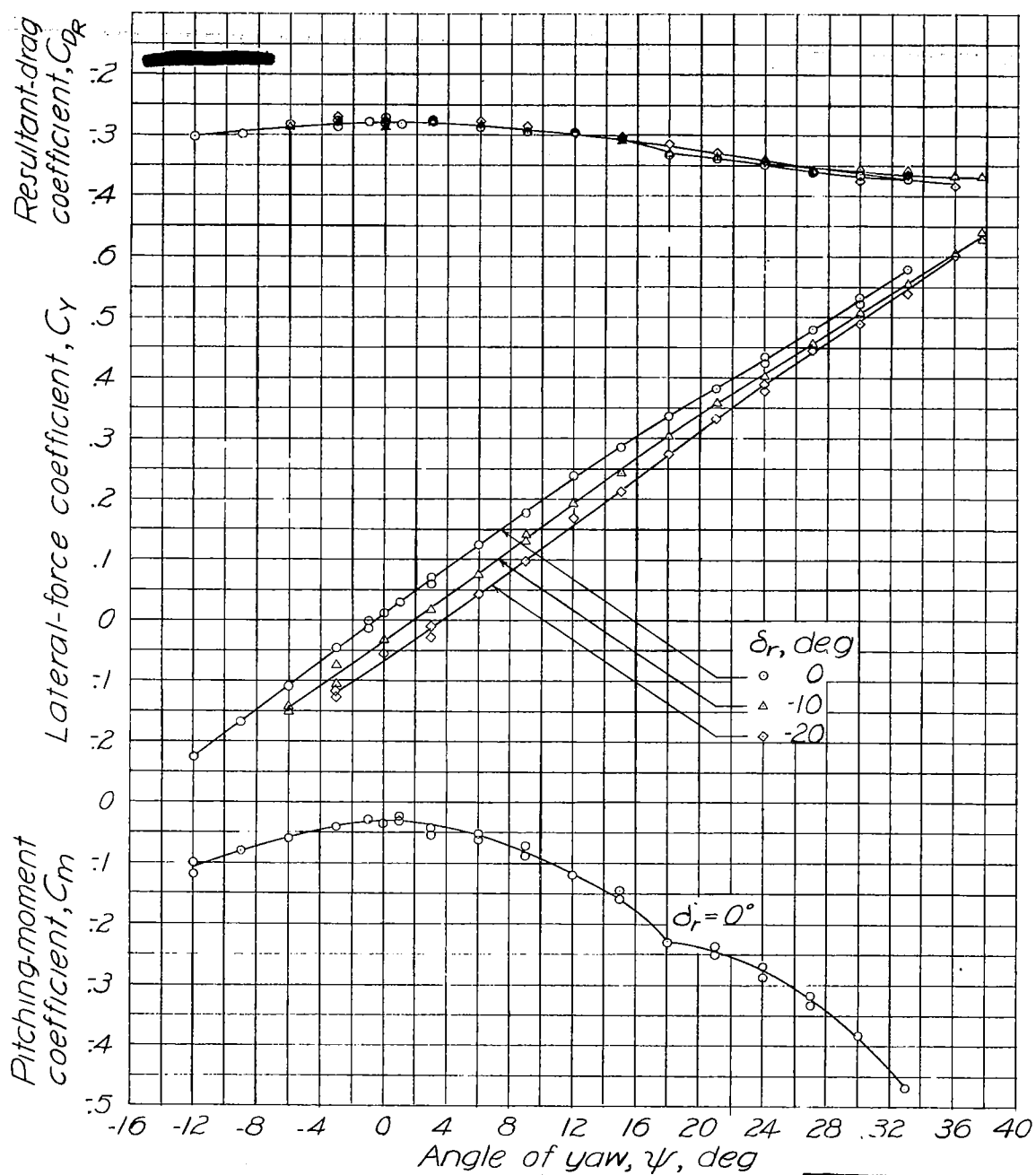


Figure 12.-Concluded.

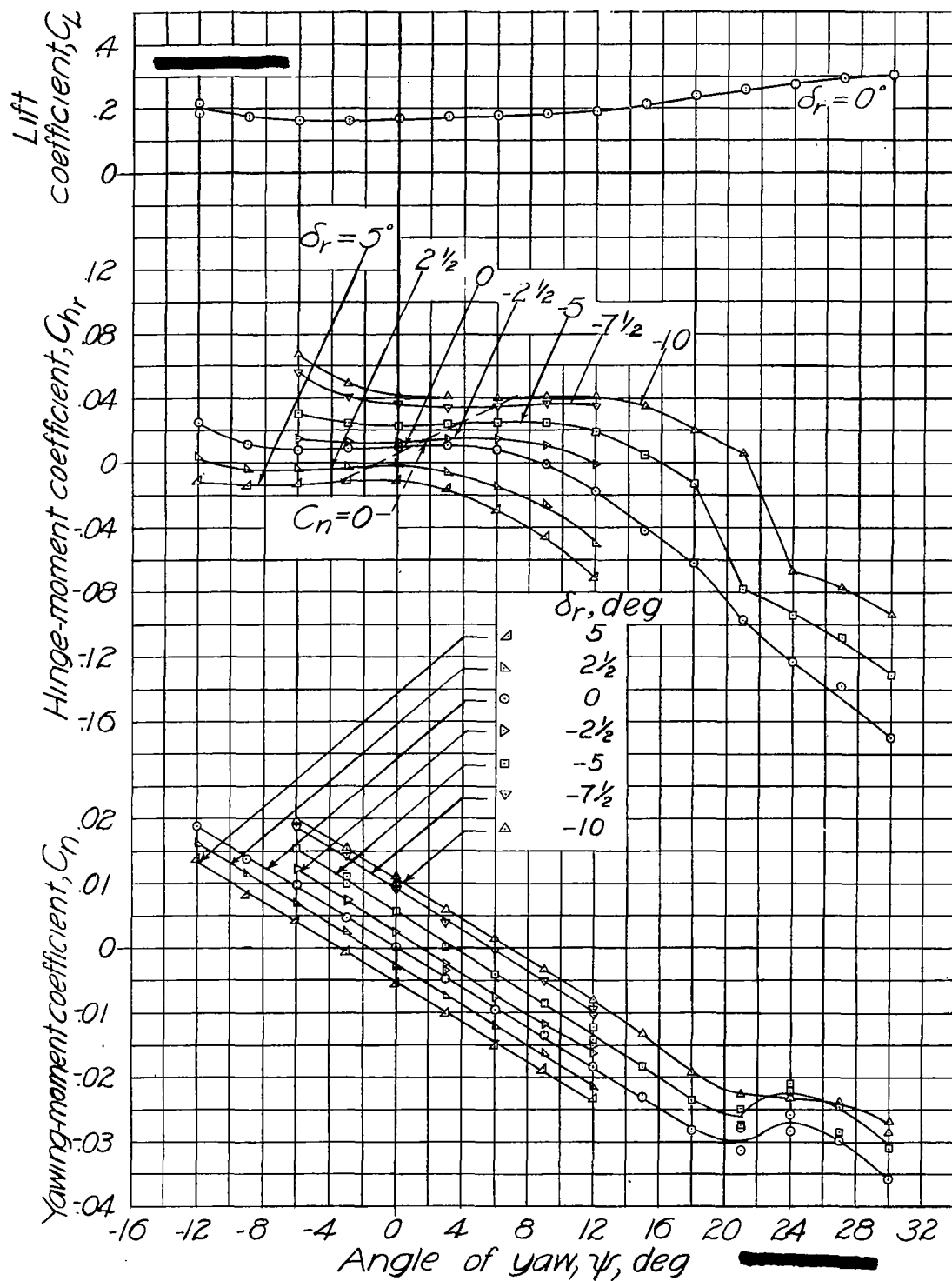


Figure 13.-Yaw characteristics for the high-speed condition. Single rotation; normal-flight configuration; full power; $T_c = 0.03$; $\alpha_T = -0.8^\circ$; $\delta_e = 0.3^\circ$; $R = 4,200,000$.

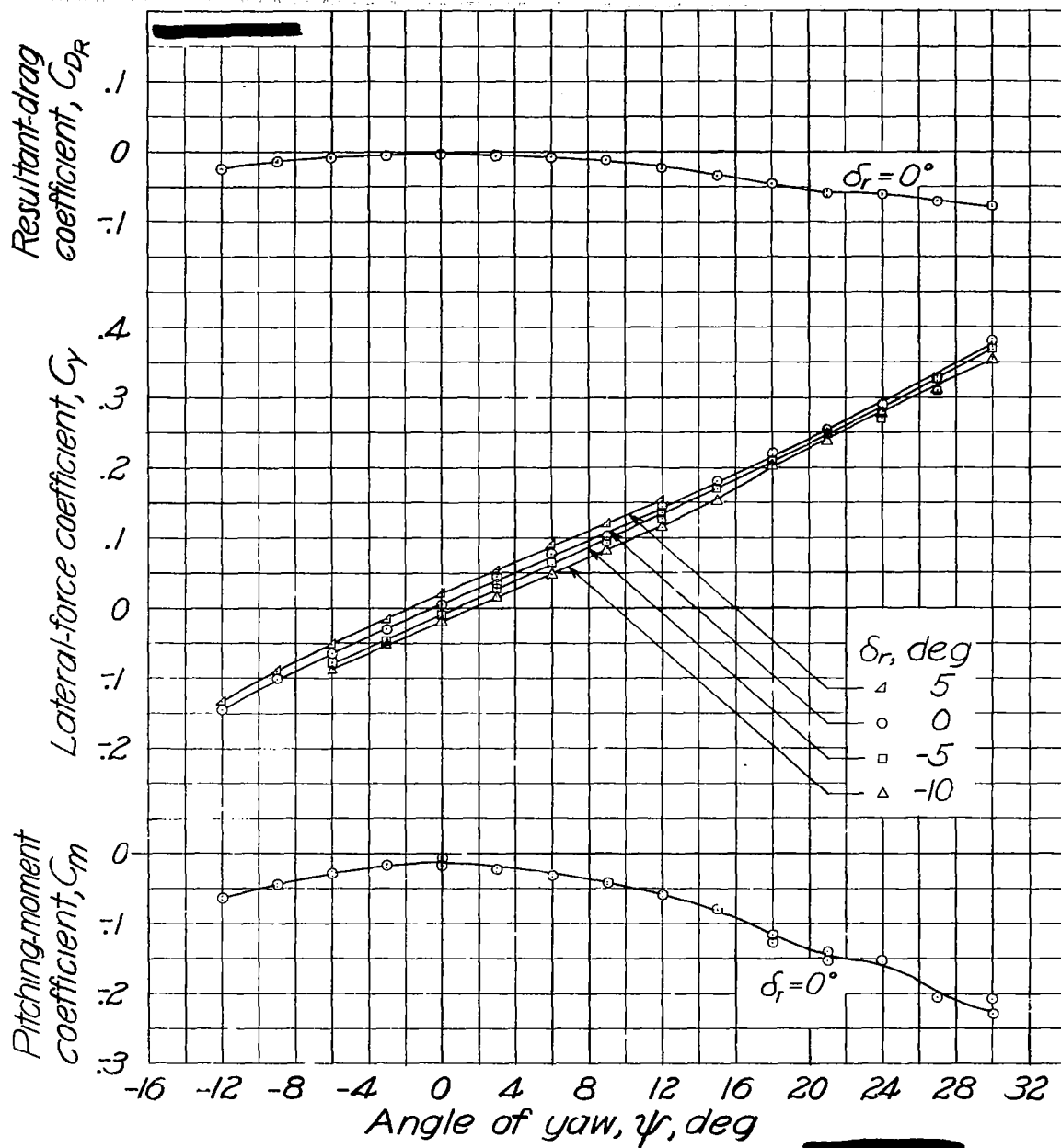


Figure 13.-Concluded.

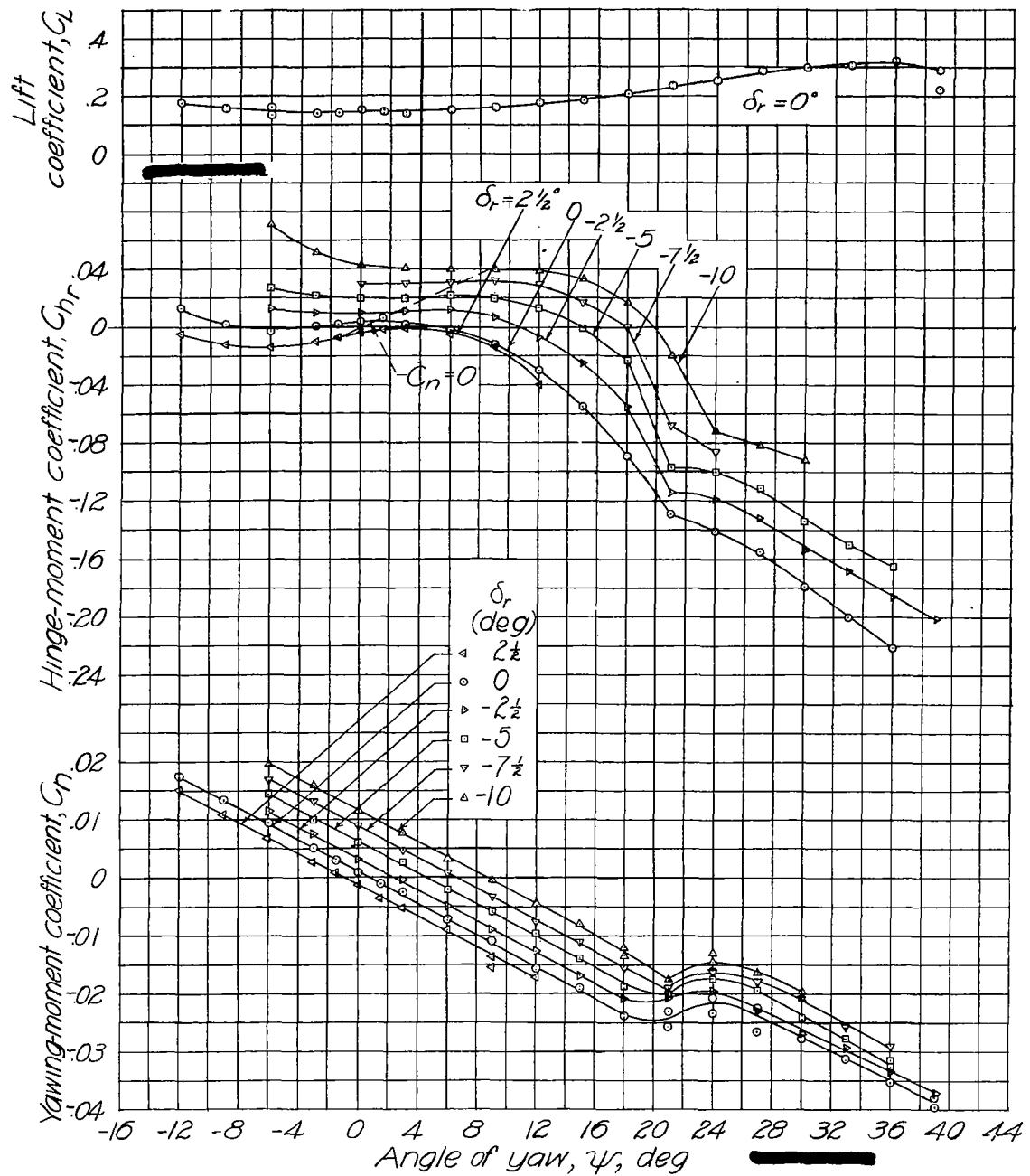


Figure 14.- Yaw characteristics for the high-speed condition. Dual rotation; normal-flight configuration; full power; $T_c = 0.03$; $\alpha_T = -0.8^\circ$; $\delta_e = 0.3^\circ$; $R = 4,200,000$.

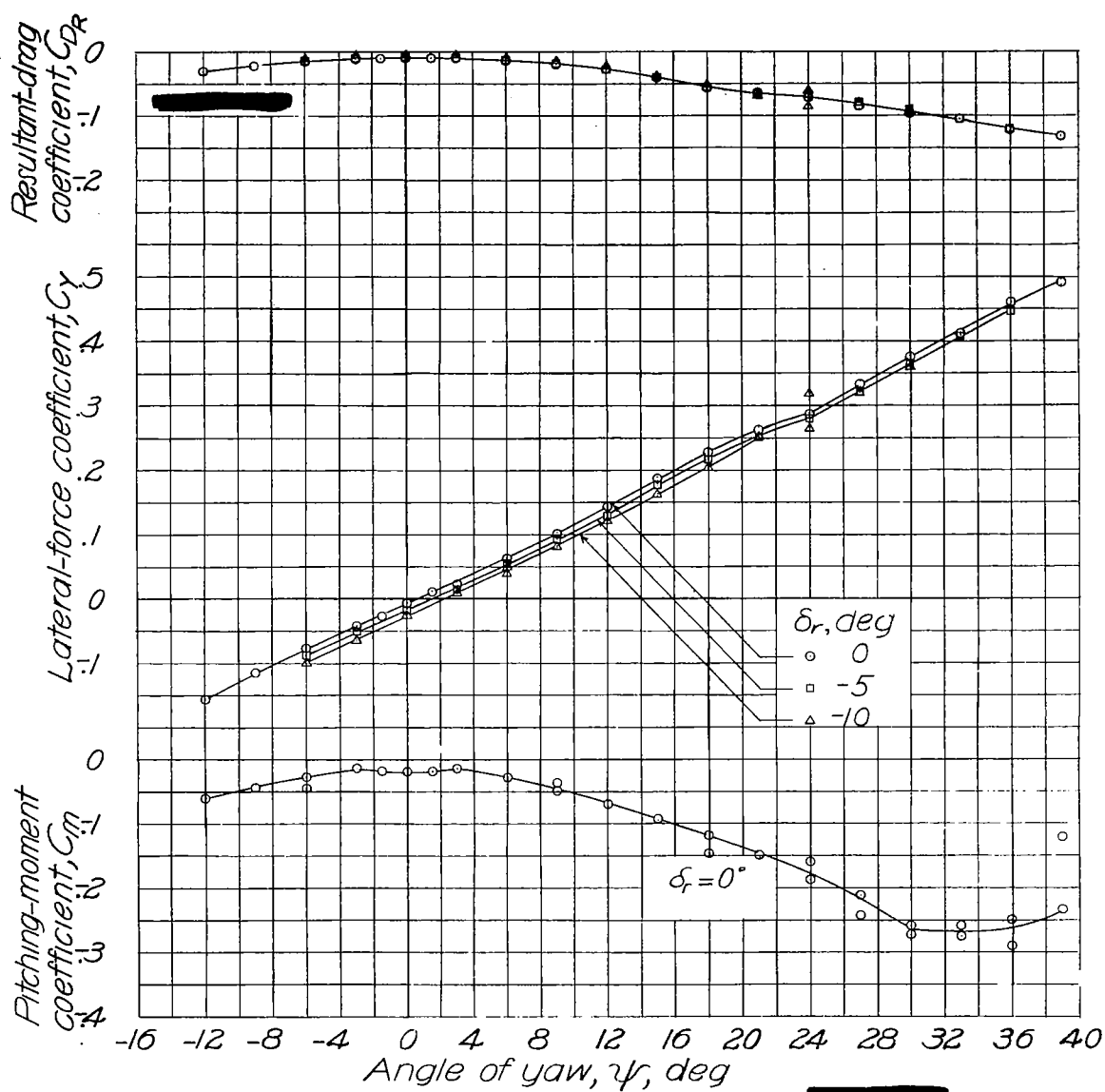


Figure 14.-Concluded.

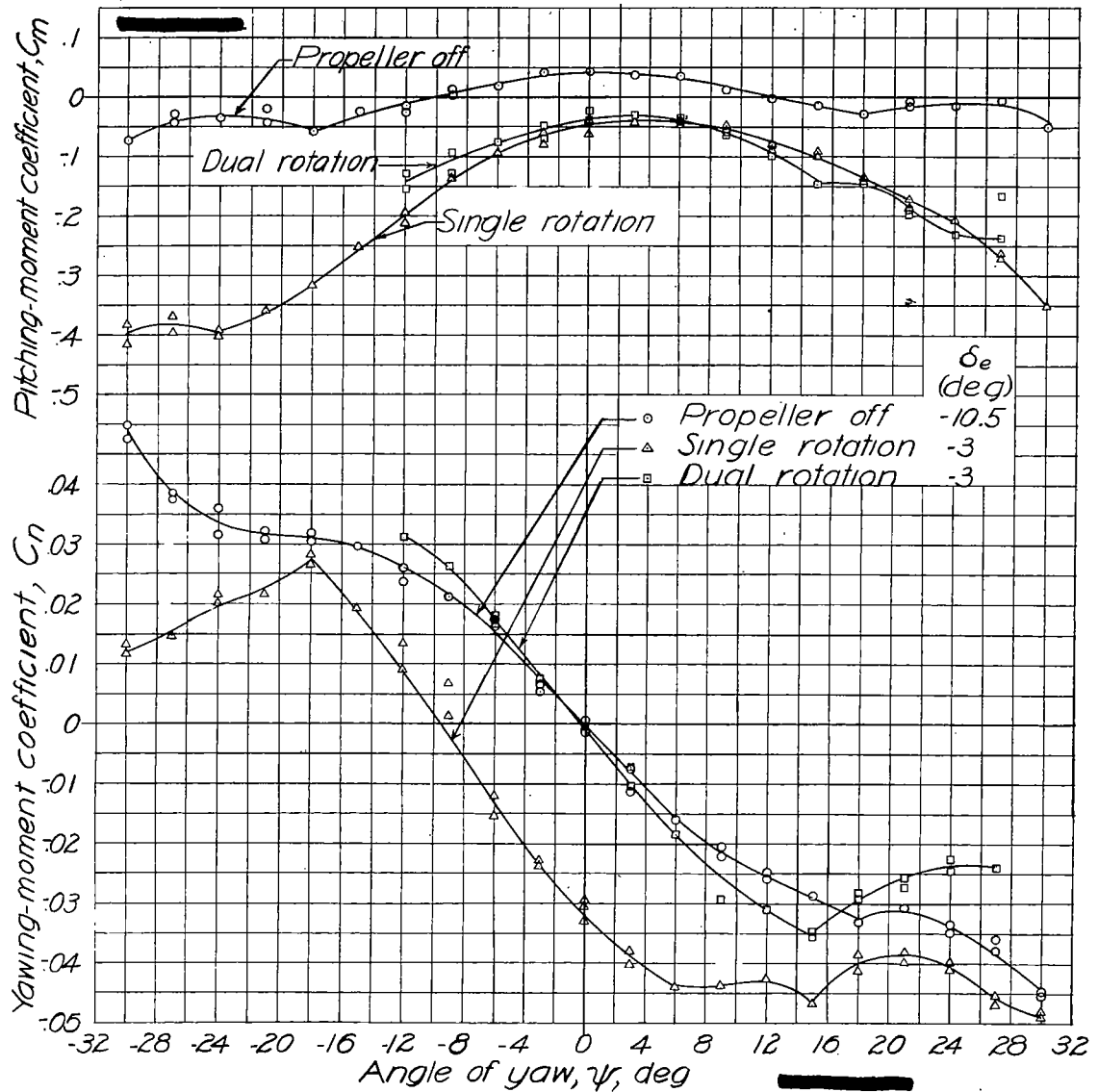


Figure 15.—Effect of rotation on yaw characteristics for the approach condition. Tail on; $\delta_r = 0^\circ$; landing configuration; 55-percent full power; $T_c = 0.59$; $\alpha_T = 10^\circ$; $R = 3,000,000$.

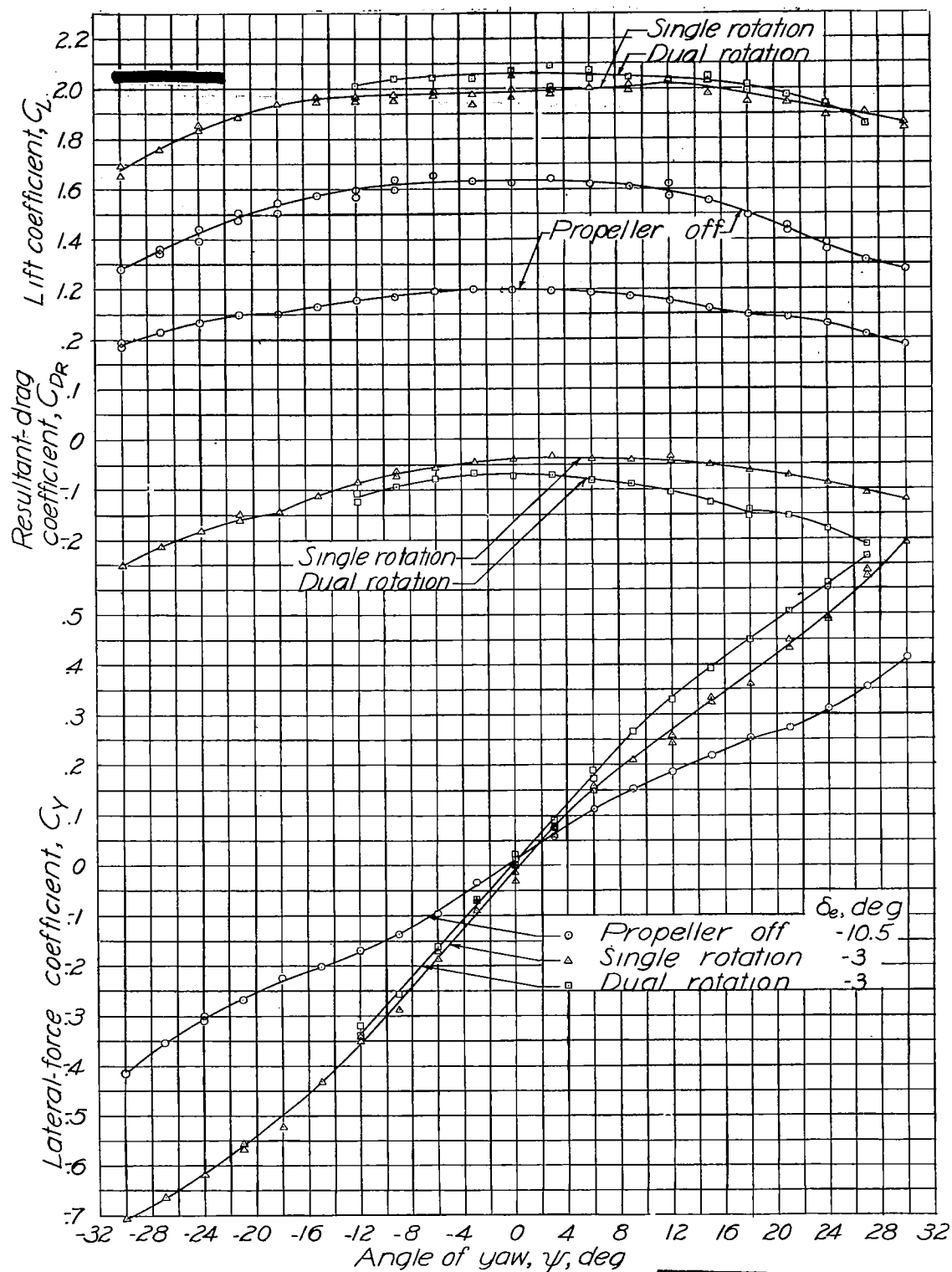


Figure 15.-Concluded

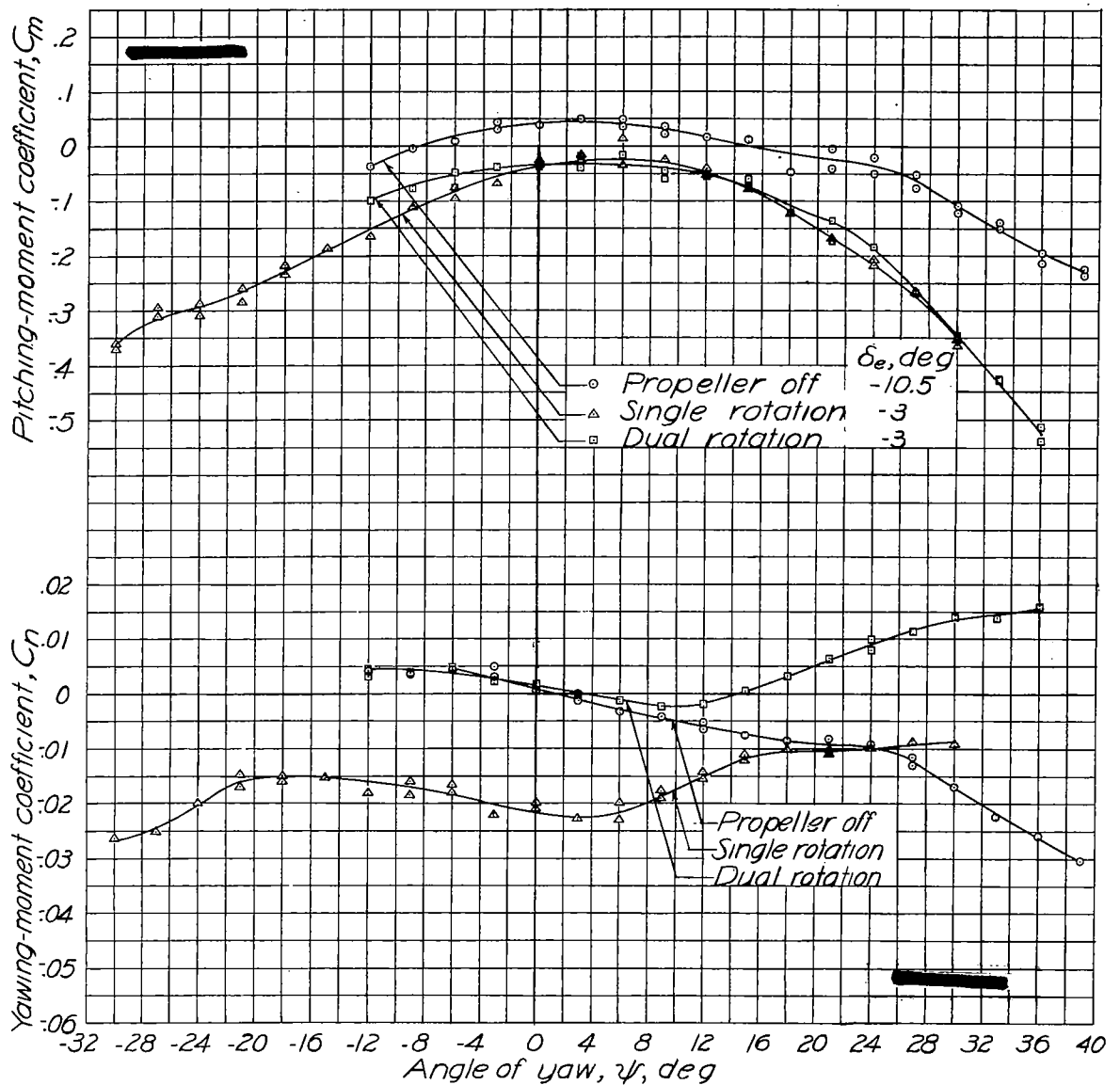


Figure 16.-Effect of rotation on yaw characteristics for the approach condition. Vertical tail off; landing configuration; 55-percent full power; $T_c = 0.59$; $\alpha_T = 10^\circ$; $R = 3,000,000$.

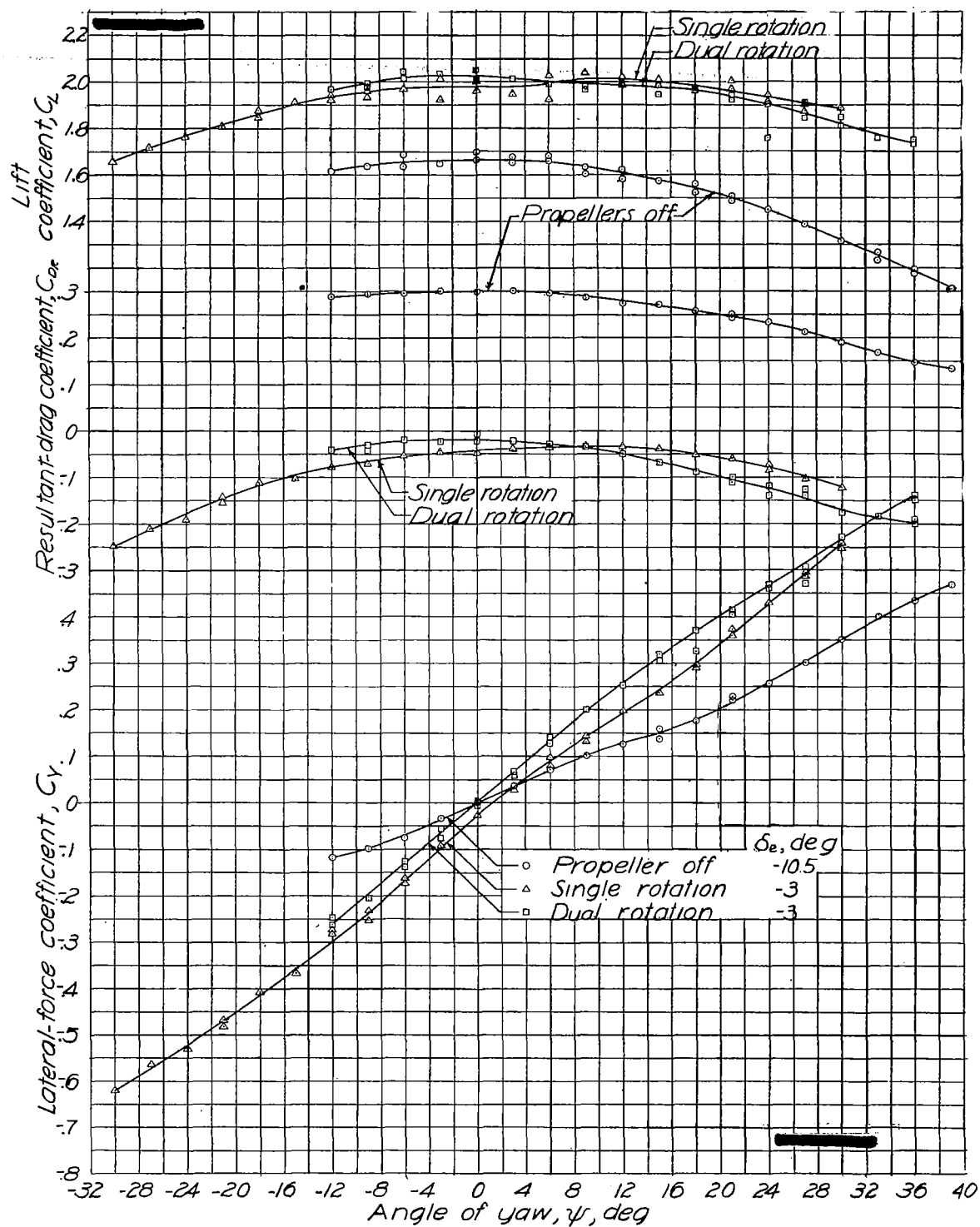


Figure 16.-Concluded

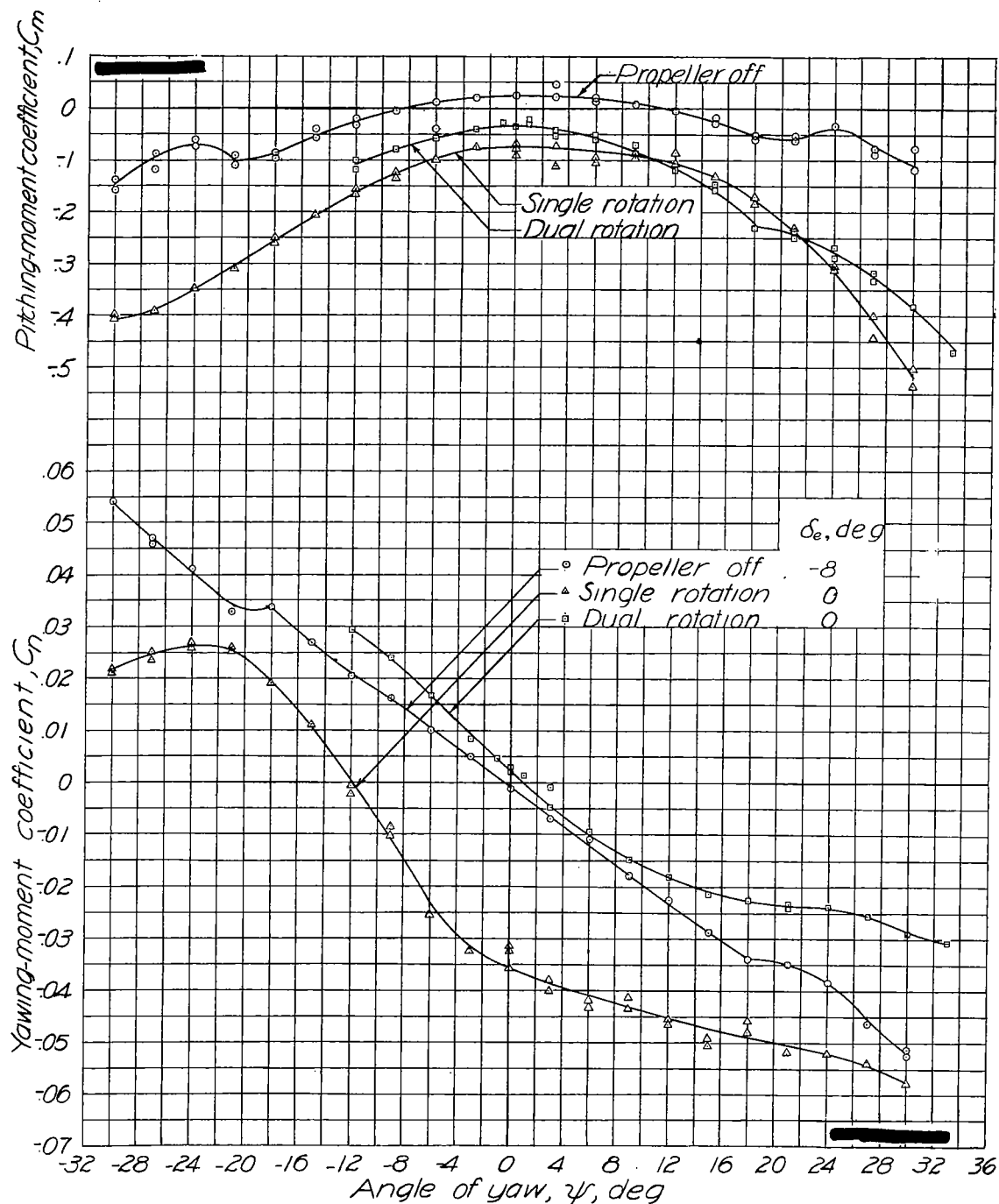


Figure 17.- Effect of rotation on yaw characteristics for the climb condition. Tail on, $\delta_r = 0$; normal-flight configuration, full power; $T_e = 0.55$, $\alpha_{cr} = 11.8^\circ$; $R = 3,000,000$.

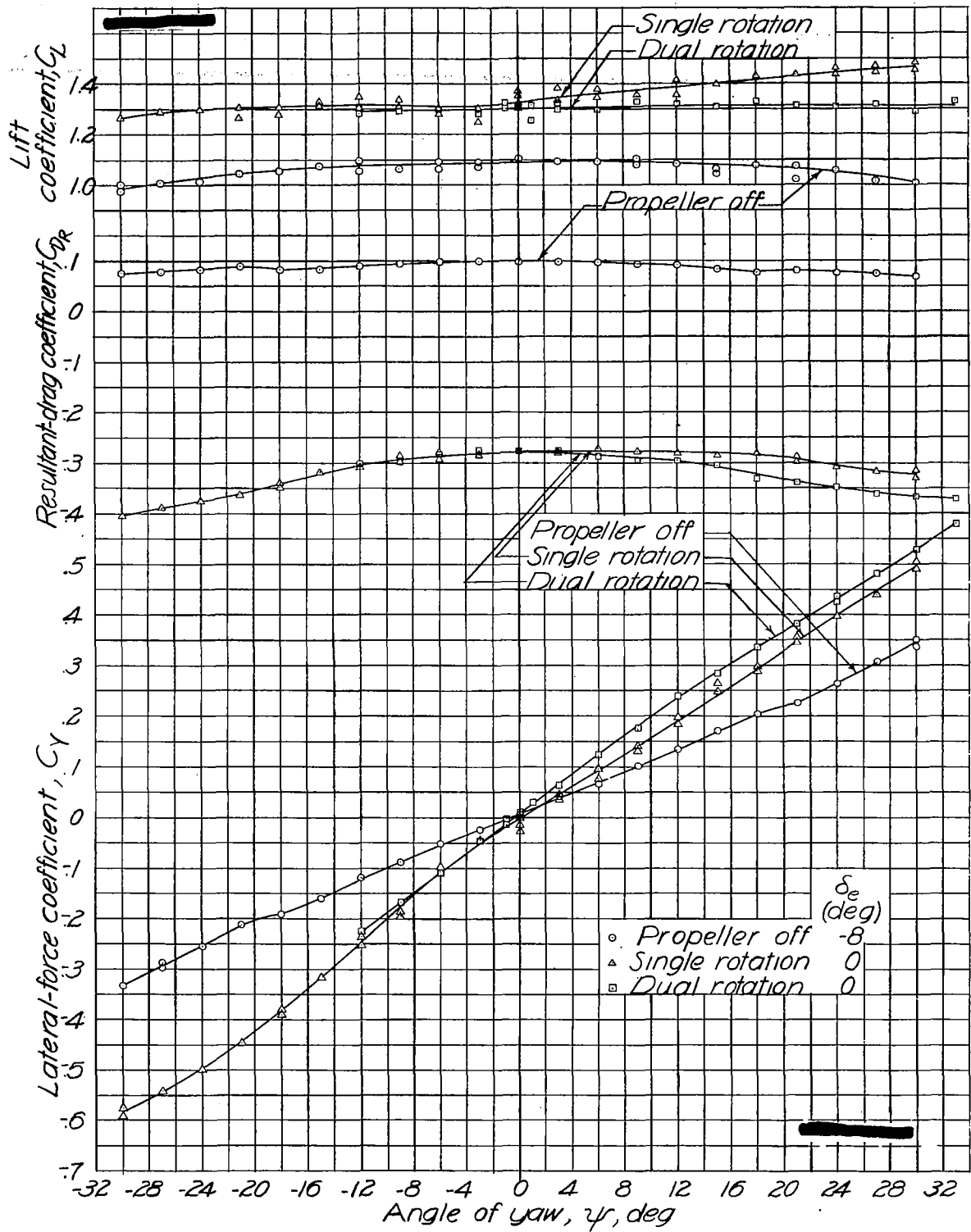


Figure 17.-Concluded.

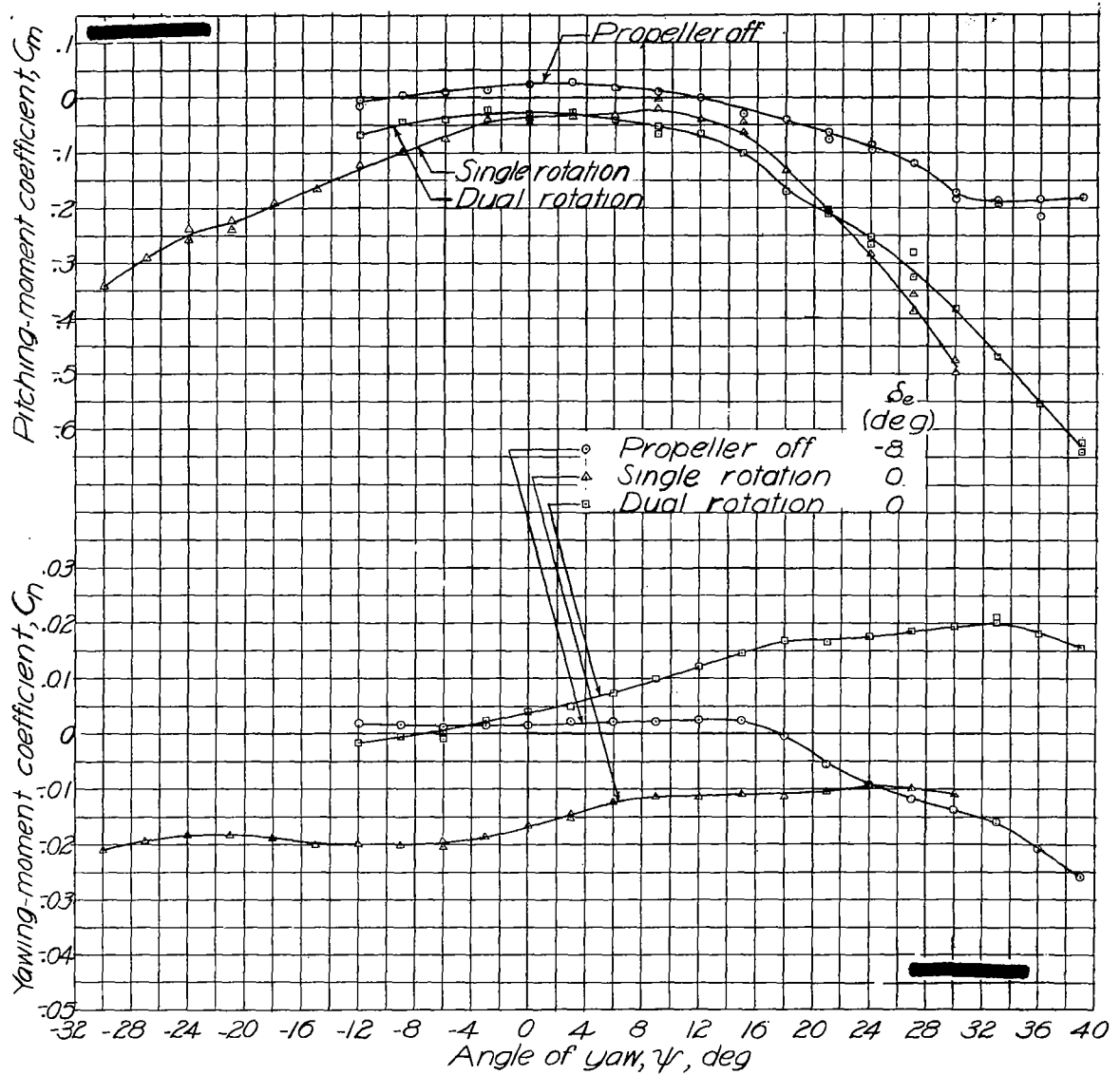


Figure 18.— Effect of rotation on yaw characteristics for the climb condition. Vertical tail off; normal flight configuration; full power; $T_c = 0.55$; $\alpha_T = 11.8^\circ$; $R = 3,000,000$.

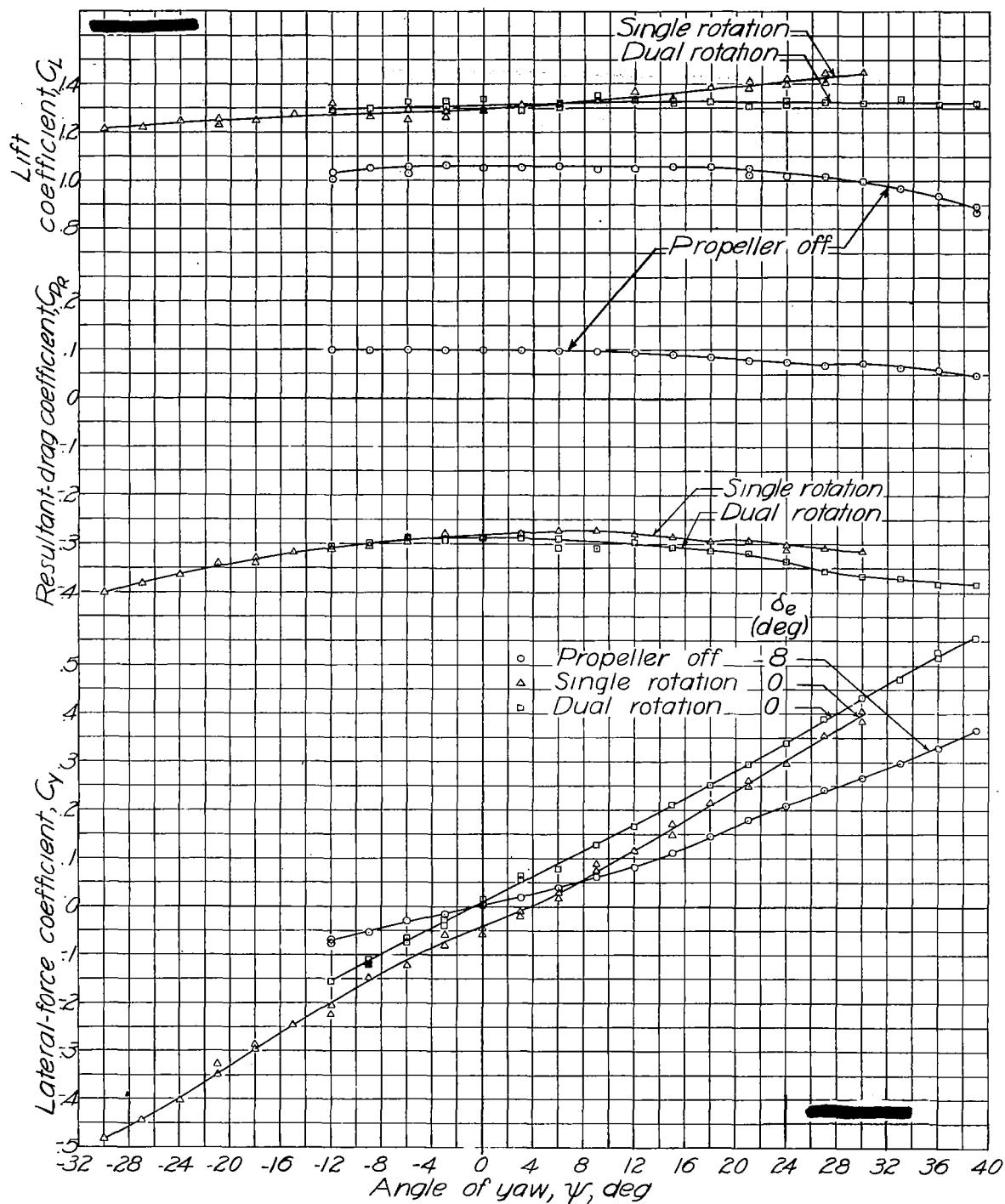


Figure 18.-Concluded.

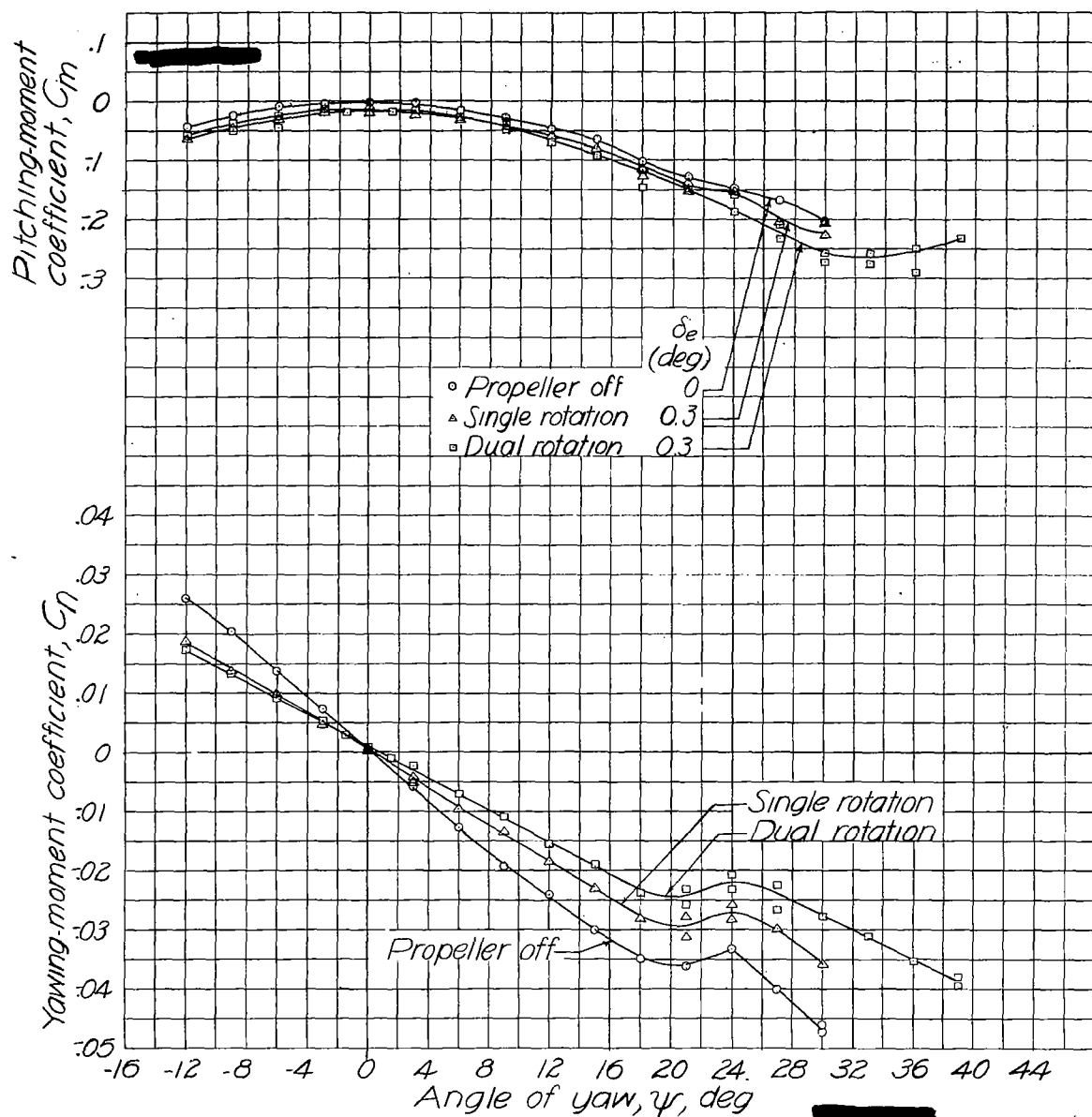


Figure 19.—Effect of rotation on yaw characteristics for the high-speed condition. Tail on; $\delta_r = 0^\circ$; normal-flight configuration; full power; $T_c = 0.03$; $\alpha_{cr} = -0.8^\circ$; $R = 4,200,000$.

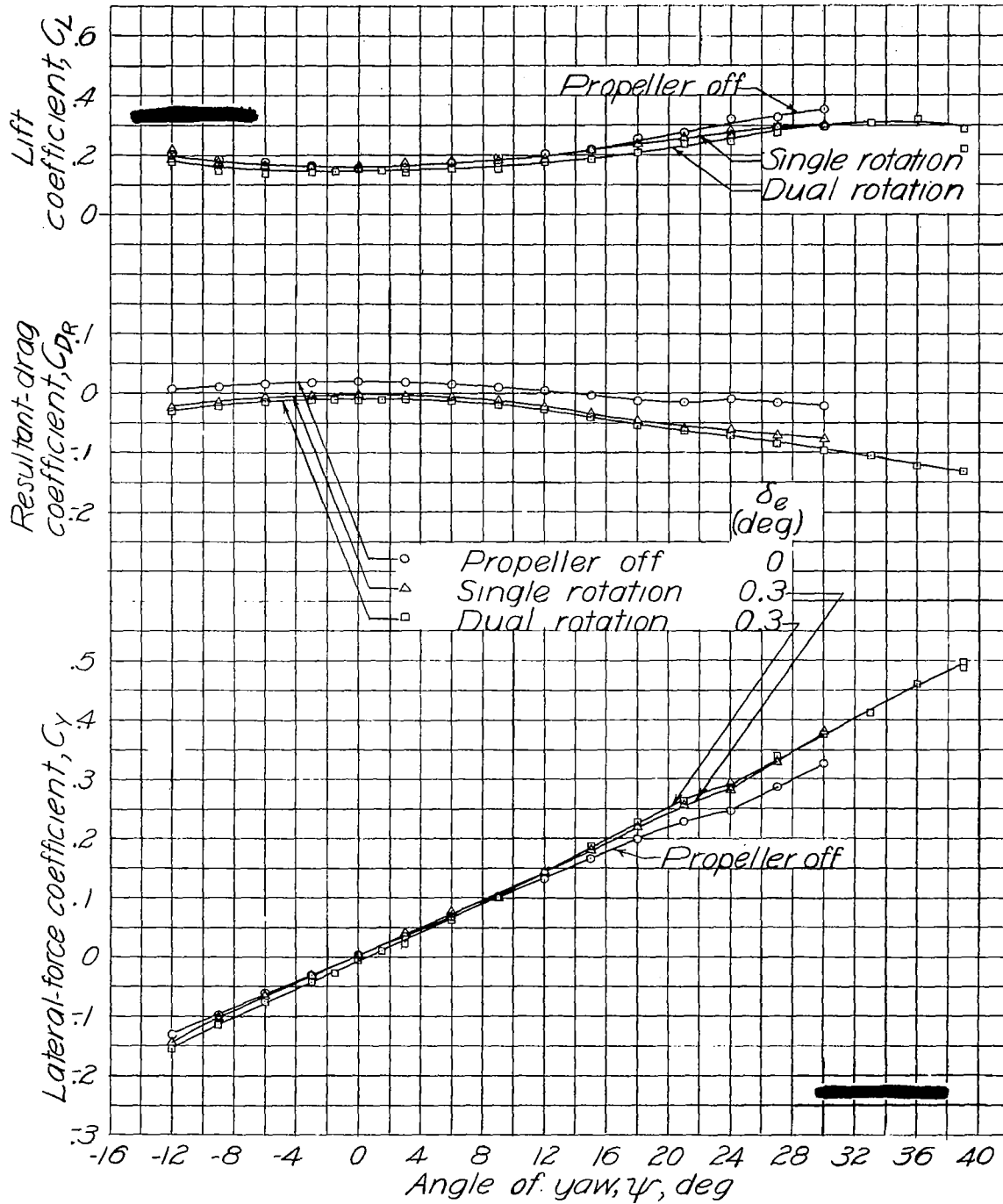


Figure 19.-Concluded.

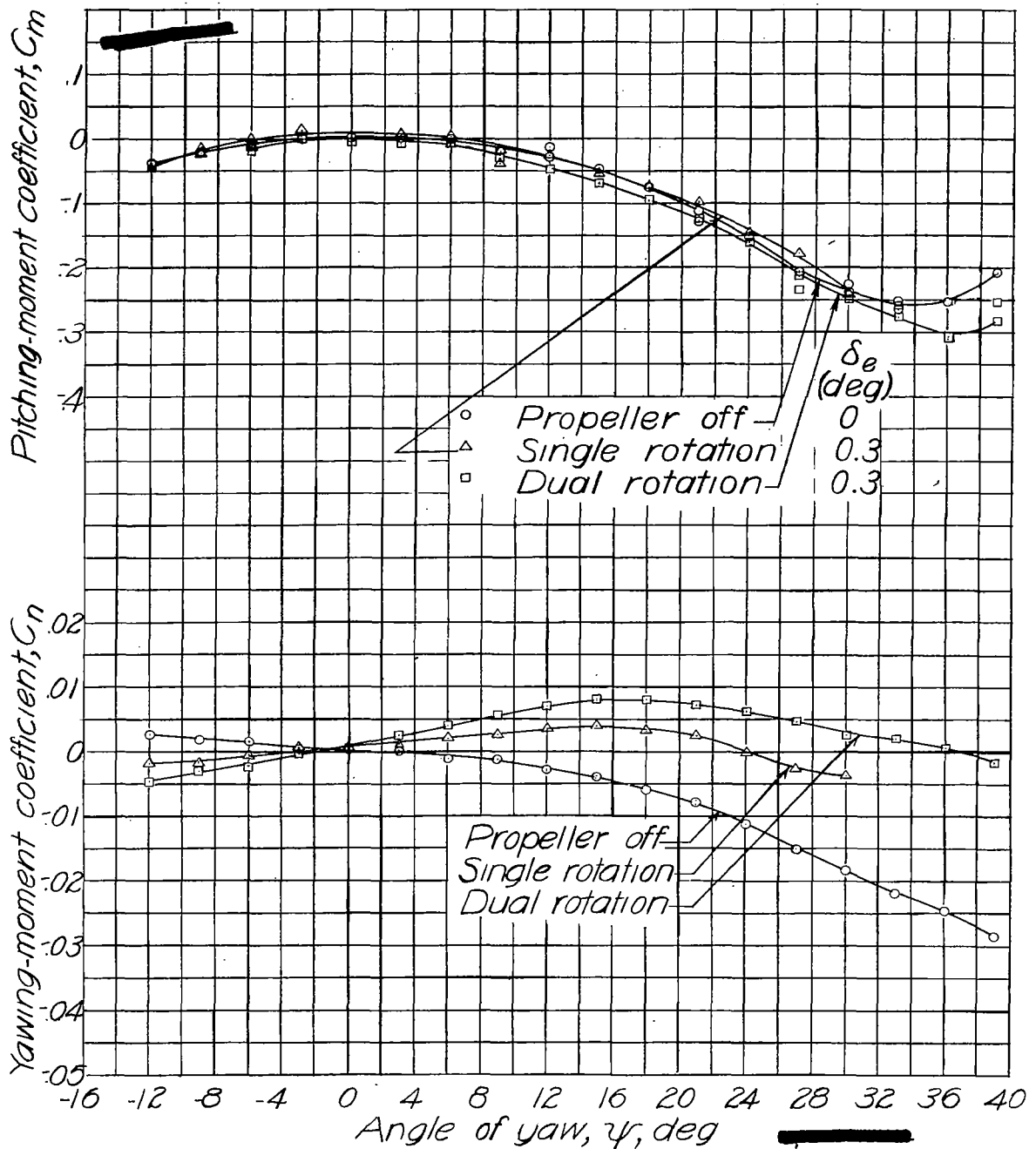


Figure 20.-Effect of rotation on yaw characteristics for the high-speed condition. Vertical tail off; normal-flight configuration; full power; $T_c = 0.03$; $\alpha_T = -0.8^\circ$; $R \approx 4,200,000$.

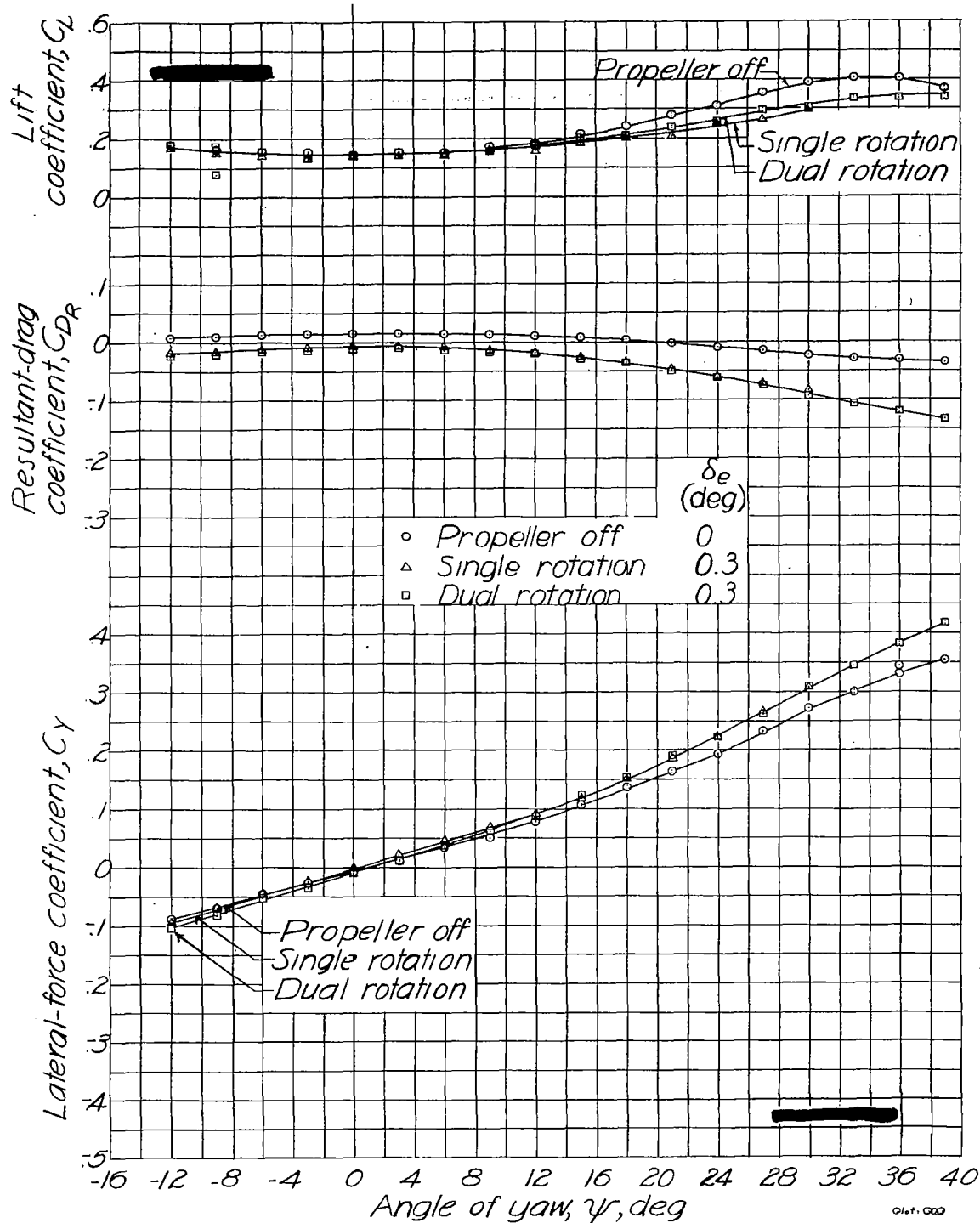


Figure 20.-Concluded.

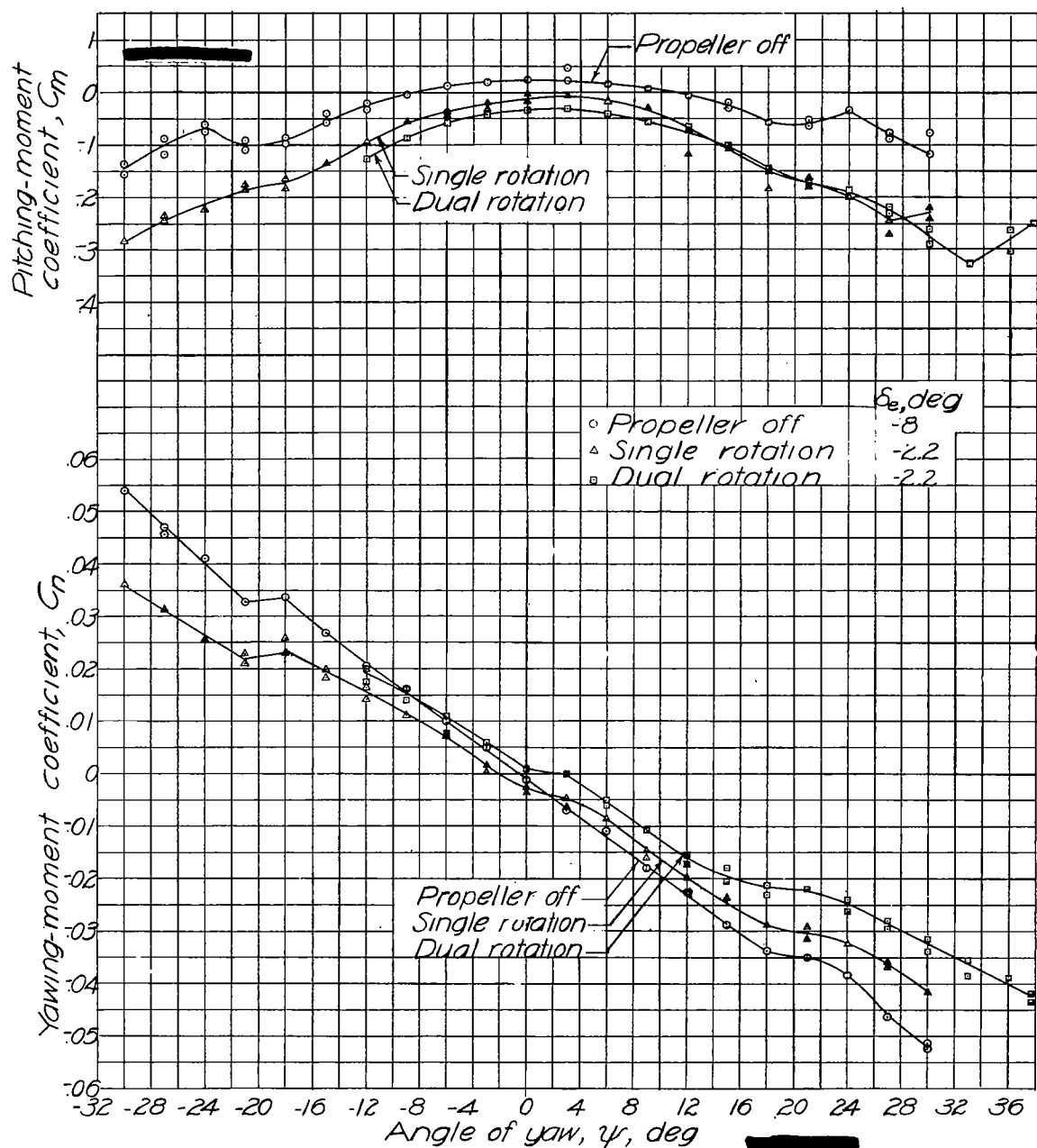


Figure 21.- Effect of rotation on yaw characteristics for the glide condition. Tail on; $\delta_r=0$; normal-flight configuration; $T_c=0$; $\alpha_T=11.6^\circ$; $R \approx 3,000,000$.

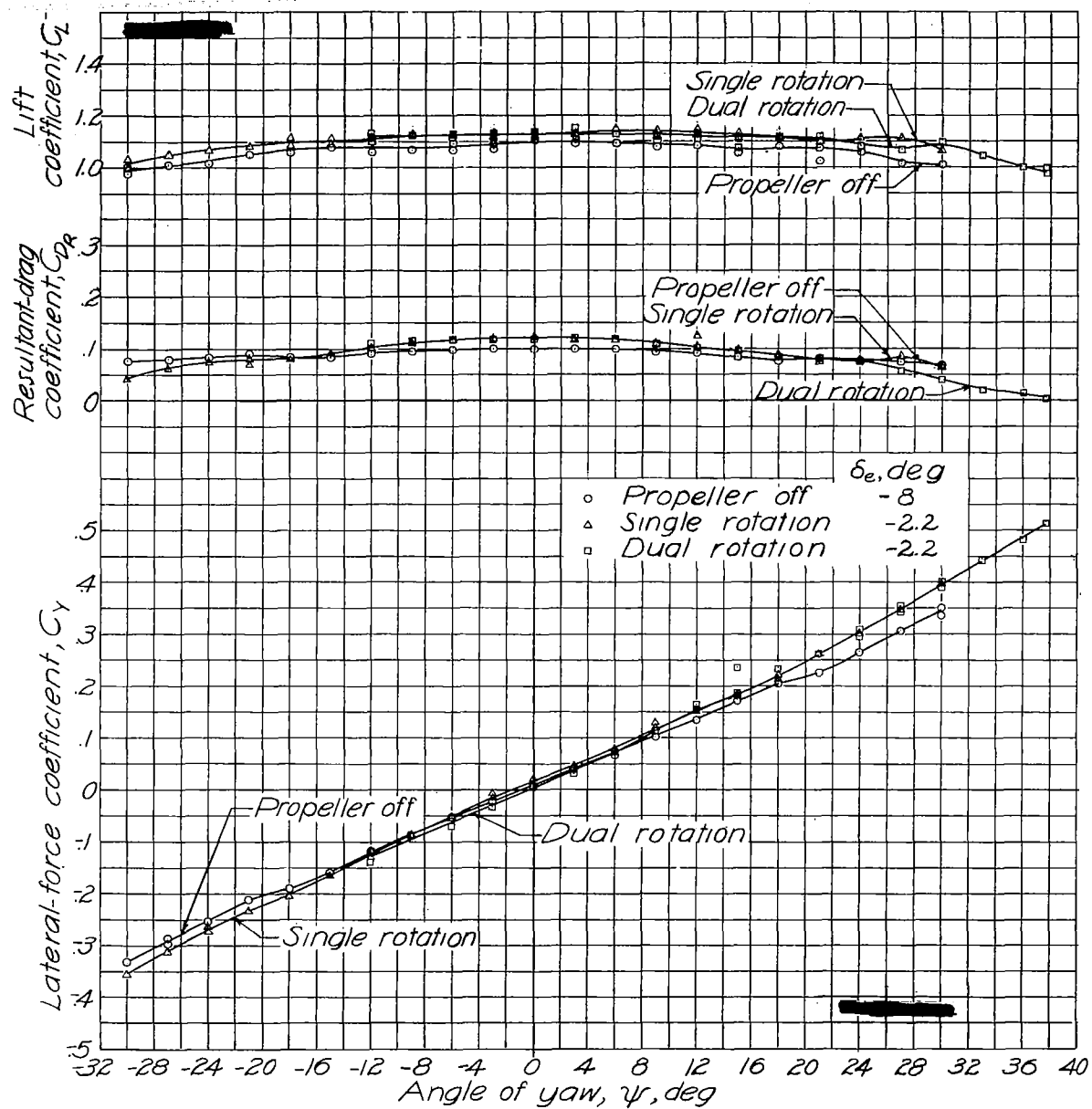


Figure 21.- Concluded.

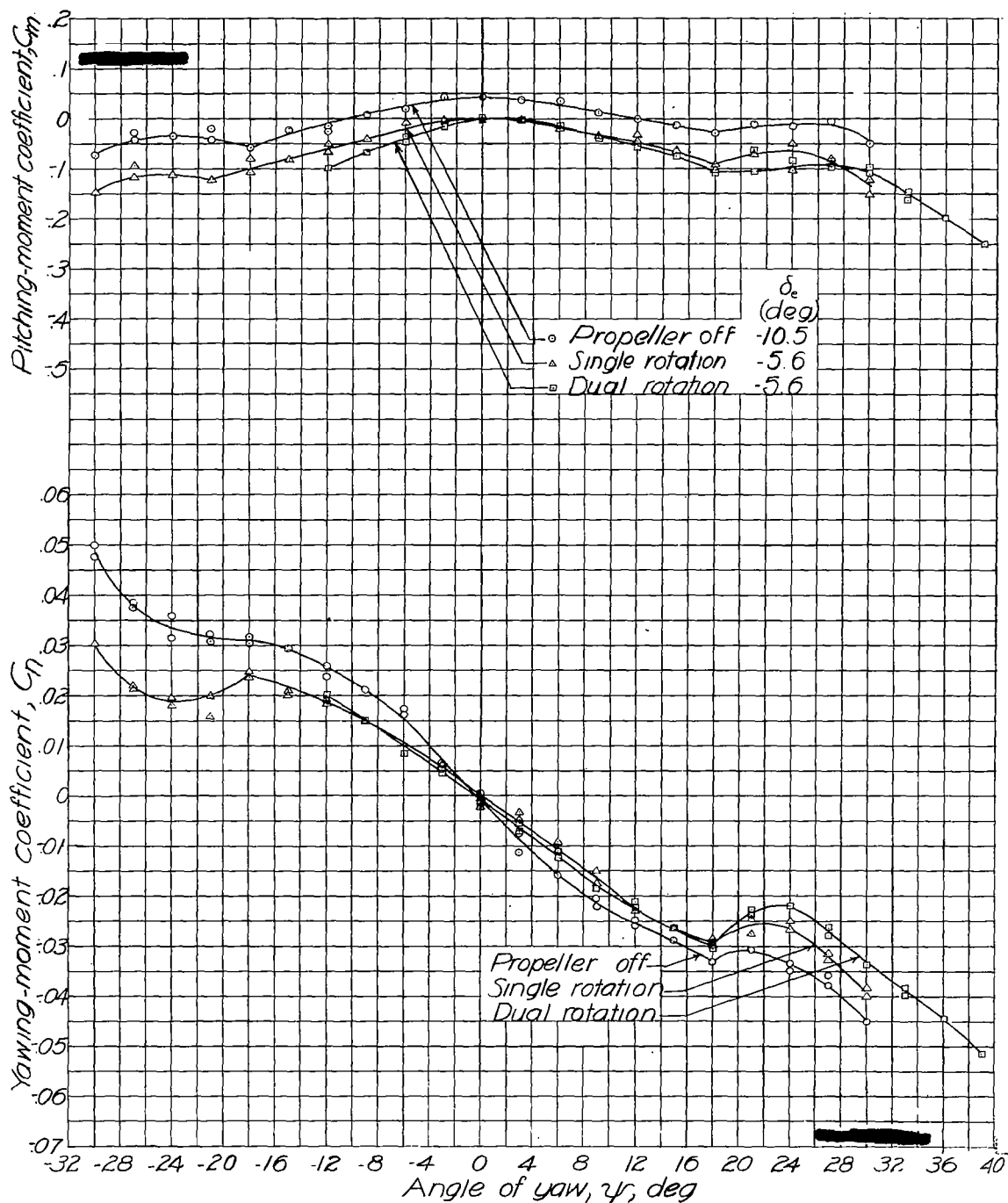


Figure 22.— Effect of rotation on yaw characteristics for the glide condition. Tail on, $\delta_t = 0^\circ$; landing configuration; $T_c = 0$; $\alpha_T = 9.7^\circ$; $R = 3,000.000$

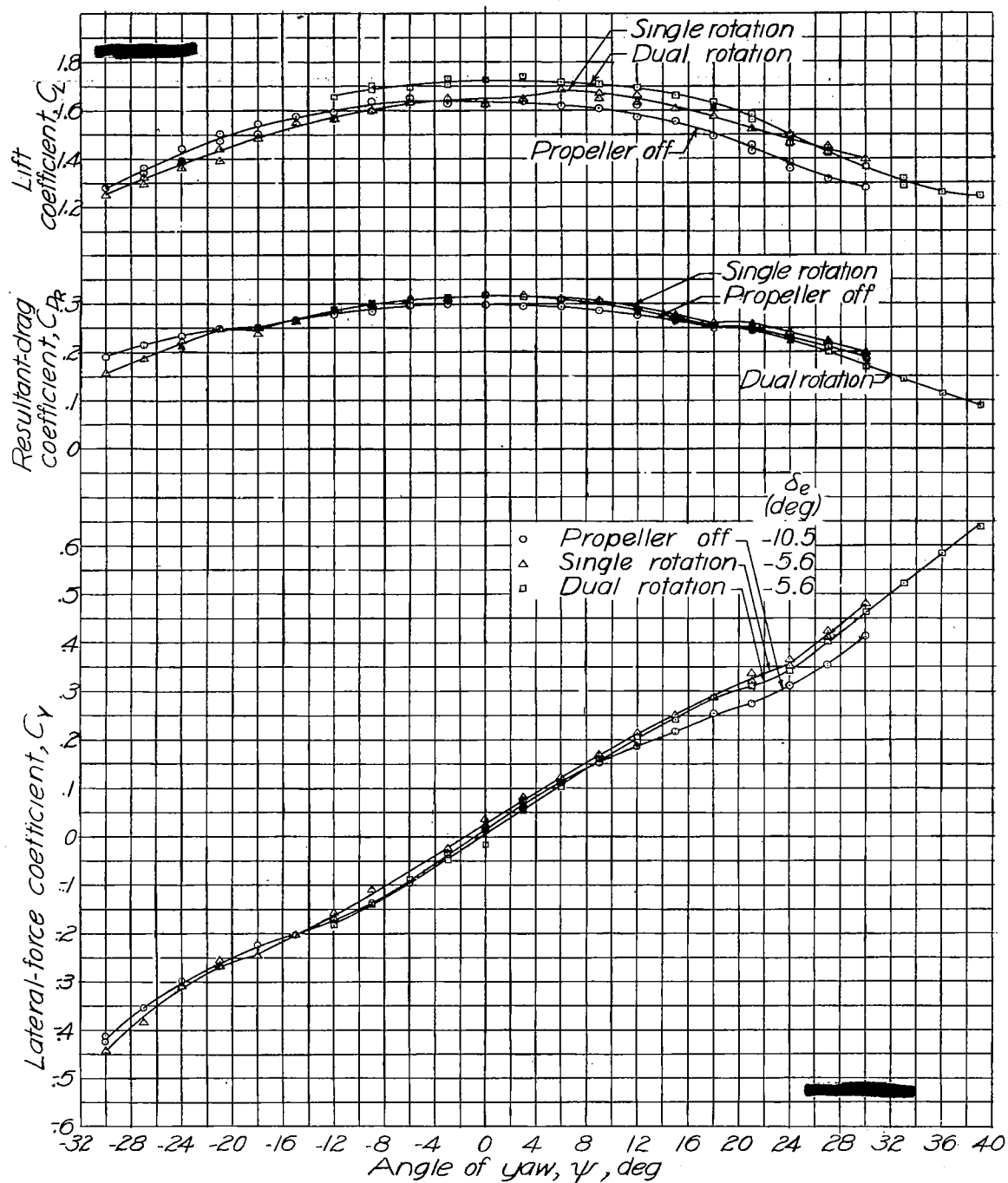


Figure 22.-Concluded

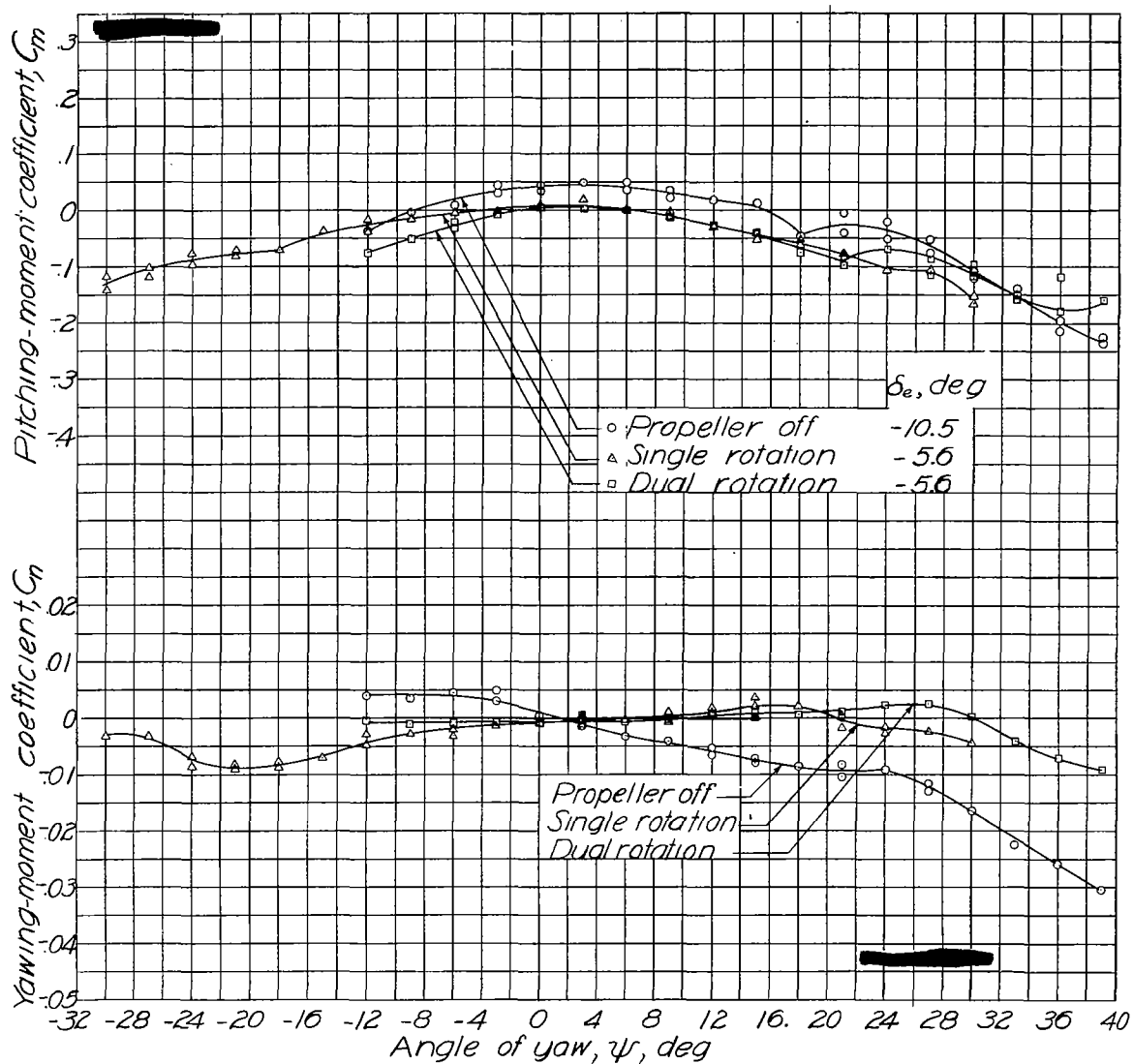


Figure 23.-Effect of rotation on yaw characteristics for the glide condition. Vertical tail off; landing configuration; $T_c = 0$; $\alpha_T = 9.7^\circ$; $R \approx 3,000,000$.

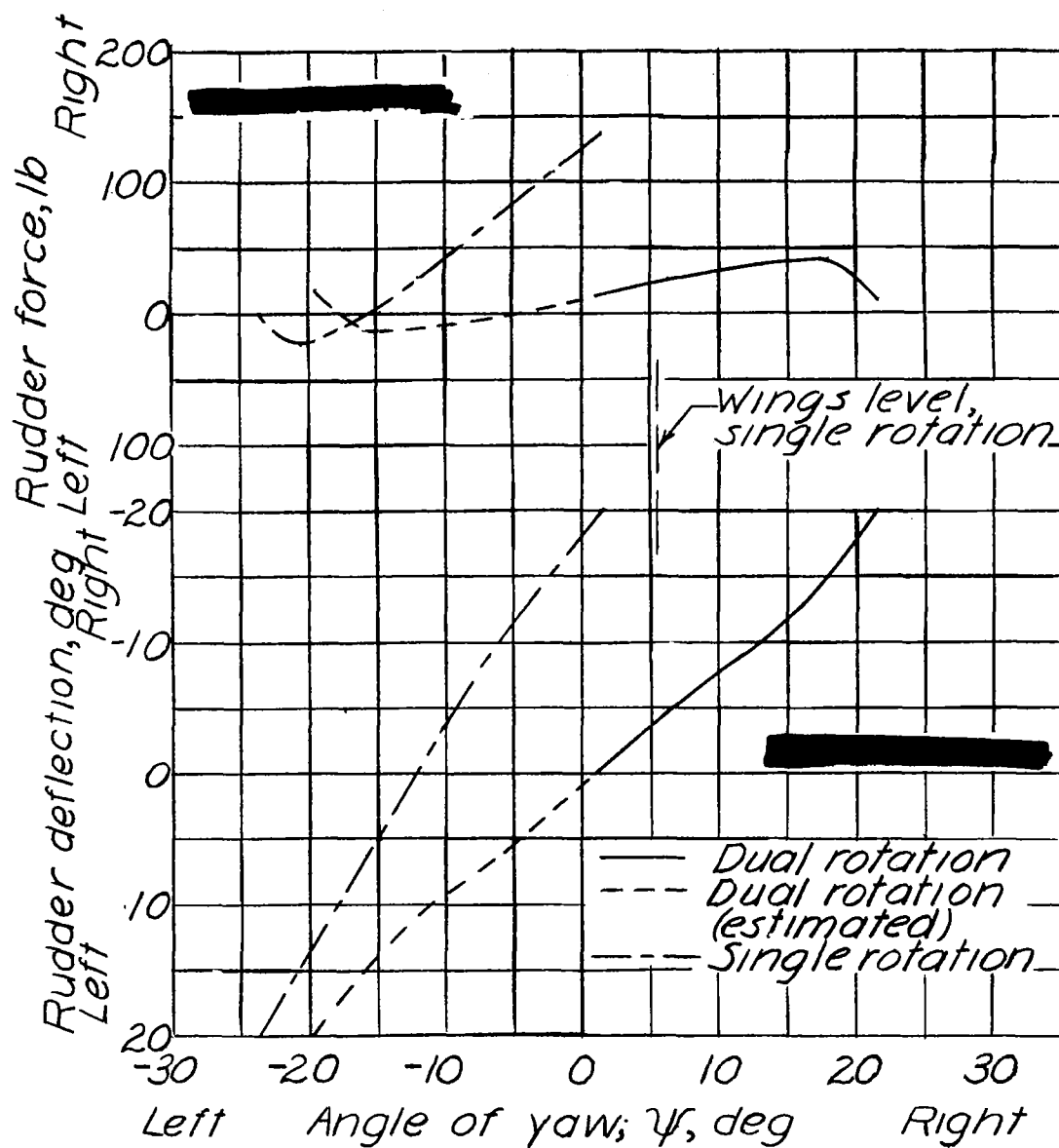


Figure 25.—Steady sideslip characteristics
($C_n=0$) for the climb condition. $V=104$ mph.

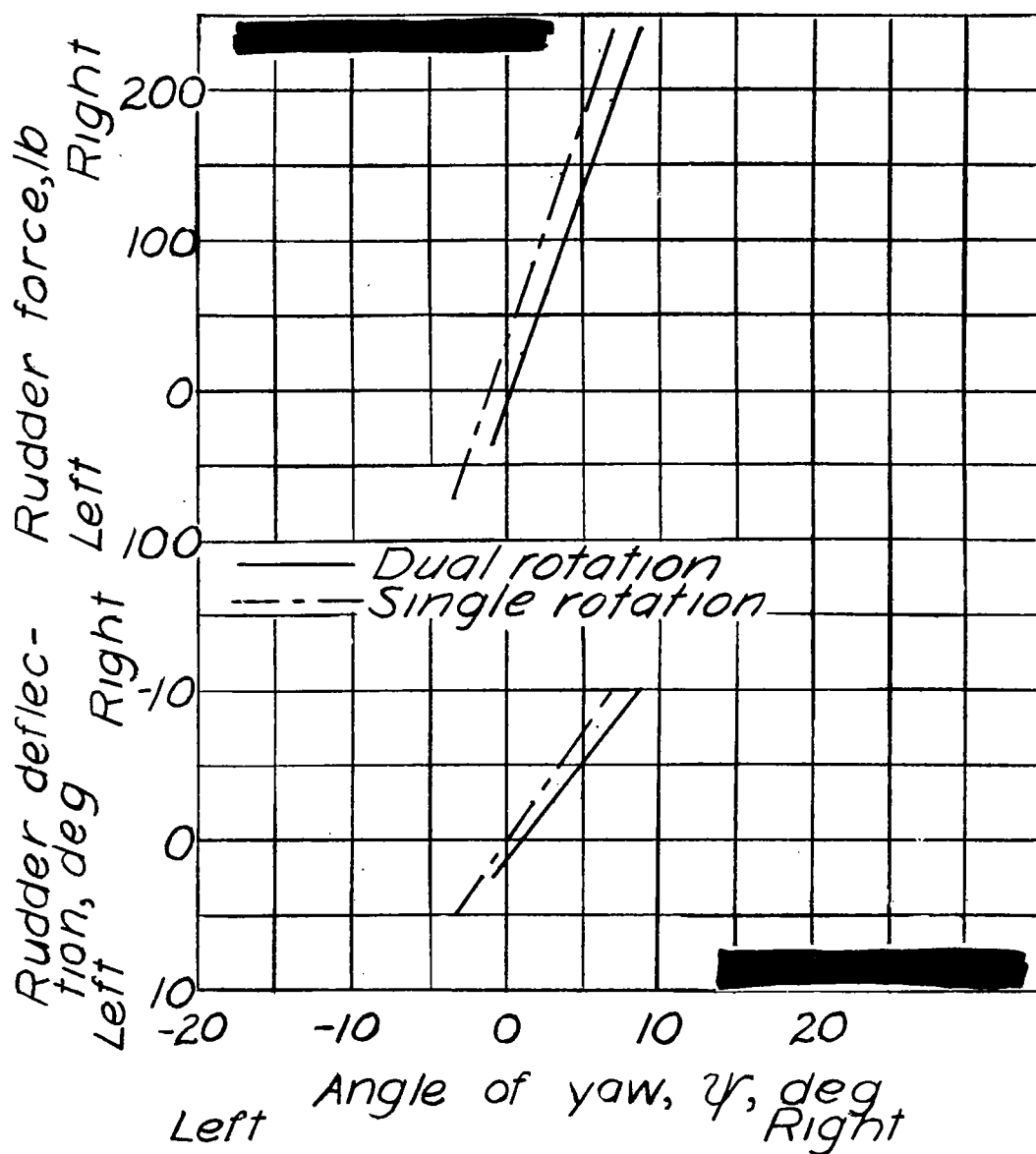


Figure 26. - Steady sideslip characteristics ($C_n=0$) for the high-speed condition. $V=306$ mph.

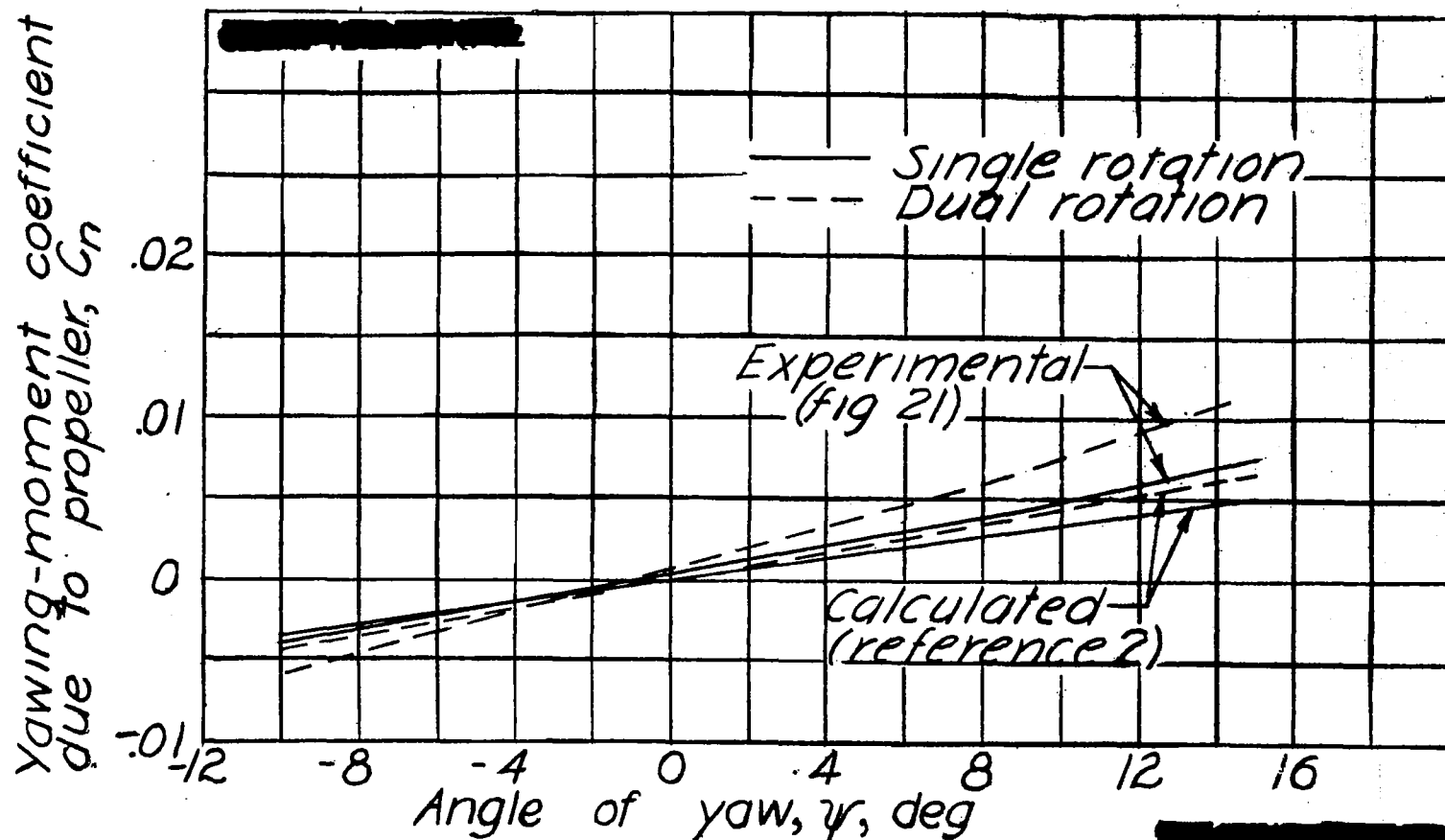


Figure 27. - Comparison of experimental and calculated yawing moments due to propeller. High-speed condition; tail off; $V/nD=1.05$; $\beta=23^\circ$.

LANGLEY RESEARCH CENTER



3 1176 01354 2064